Towards Structural Health Monitoring in Carbon Nanotube Reinforced Composites

by
Wennie Wang

Submitted to the Department of Materials Science and Engineering in Partial Fulfillment of the Requirements for the Degree of

Bachelor's of Science in Materials Science and Engineering
at the

Massachusetts Institute of Technology

June 2013

Signature of Author: _____

Department of Materials Science and Engineering
May 3, 2013

Co-certified by: _____

Brian L. Wardle
Associate Professor of Aeronautics and Astronautics
Co-Thesis Supervisor

Co-certified by: _____

Jeffrey C. Grossman
Carl Richard Soderberg Associate Professor of Power Engineering
Co-Thesis Supervisor

Accepted by: _____

Jeffrey C. Grossman
Chairman of the DMSE Undergraduate Committee

Towards Structural Health Monitoring in Carbon Nanotube Reinforced Composites

by
Wennie Wang

Submitted to the Department of Materials Science and Engineering on May 3, 2013 in Partial Fulfillment of the Requirements for the Degree of

Bachelor's of Science in Materials Science and Engineering
at the

Massachusetts Institute of Technology

ABSTRACT

An experimental investigation was conducted to understand the non-destructive evaluation (NDE) capabilities of carbon nanotubes (CNTs) of several network architectures towards structural health monitoring (SHM). As heterogeneous composite structures become increasingly common in industry, detecting mechanical damage and damage accumulation becomes increasingly difficult as many modes of failure occur below the external surface. Traditional SHM techniques may be time consuming and costly; however, CNTs are a unique material that shows promise as a strain or damage sensor. Three different laminate samples types with various CNT network architectures were tested in open-hole tension. Samples tested were quasi-isotropic carbon fiber, carbon fiber prepreg with unidirectional knocked-down CNT surface patch, and fuzzy fiber reinforced plastic (FFRP) samples, which consist of radially grown CNTs on a woven ceramic fiber substrate.

Mechanical load and electrical resistance were simulataneously measured using three different probes configurations with respect to the tensile direction that measured either surface or through thickness resistance changes. Measurements were taken near and away from the stress concentration. Results indicated that different CNT network architectures influenced the consistency and efficacy of indicating damage acculumation. Changes in electrical resistance correlated strongly with sample mechanical damage accumulation for unidirectional knocked-down CNTs, but had more consistent values and readings for the FFRP samples, indicating that CNT network architecture beyond the inherent piezoresistivity of the CNT heavily influences the NDE capabilities of using CNTs as strain or damage sensors. Results also suggest that CNT network architecture must be further optimized to achieve reliable NDE and SHM, and may depend on the desired application.

Primary Thesis Supervisor: Brian L. Wardle
Title: Associate Professor of Aeronautics and Astronautics

Thesis Co-Supervisor: Jeffrey C. Grossman
Title: Carl Richard Soderberg Associate Professor of Power Engineering

Contents

List of Figures

1 Introduction

Composites are materials that combine two or more materials heterogeneously such that the overall structure has the advantageous properties of each material. Depending on the desired properties, the materials may be combined in many geometrical variations, ranging from aligned fiber inclusions in a matrix to randomly distributed particles in a matrix. Aerospace composites combine very strong and stiff fibers with a compliant matrix to create unique materials with large advantages, such as strength, stiffness and minimal weight. Common aerospace composites often involve layering materials of various types in different orientations or combining two vastly different material in strategic architectures. An example is Fig. 1, in which a lightweight honeycomb structure is sandwiched between stiffer plates and creates a structure similar to that of an I-beam that is more resistant to bending. Recent research in aerospace composites has included the incorporation of various smaller materials, such as carbon nanotubes, glass fibers, or particles, dispersed throughout a polymer matrix. Such combinations typically include a stiffer material incorporated in a more compliant matrix, and result in stiffer, stronger, and tougher materials than the individual material components alone.

Figure 1: Example of honeycomb sandwich composite used commonly in aerospace structures [2].

Although structures like those shown in Fig. 1 are a marked improvement from its separate constituents, further engineering at the nano-scale is necessary to push aerospace materials further. Despite these advantages, composites are still vulnerable to failure such as delamination and fiber pull out. These modes of failure compromise the structural integrity of the material, but are often not typically visible on the surface. Thus, it is desirable to monitor the mechanical health of a structure non-invasively. Such structural health monitoring is thus desired for continued safe operation of composites in aerospace applications. Although many materials have been used as sensors in the field of structural health monitoring, the focus of this investigation is carbon nanotubes (CNTs) as mechanically reinforcing and self-sensing materials in aerospace composite applications as materials for non-destructive evaluation in working towards structural health monitoring.

1.1 An Overview of Structural Health Monitoring and Damage Sensing in Composites

Structural health monitoring (SHM) is the idea of monitoring the mechanical integrity of a part during operation in real time non-destructively. Due to the heterogeneous structure in composites, damage, such as delamination between layers, fiber breakage, fiber pullout, or fiber debonding, is often below the surface of the structure and so cannot be immediately detected using traditional methods (e.g. visual inspection). Similarly, non-destructive evaluation (NDE) is a subform of SHM in which the integrity of a structure is evaluated out of operation and system acquisition is done outside the sample or structural part. CNTs as structural health monitoring materials is still under development in various systems, and therefore the scope of this investigation is NDE of CNT reinforced composites. Many different material candidates have been considered for structural health monitoring, such as CNTs (see Section 1.3) for their changes in resistance with mechanical load and metallic alloys for their change in magnetic susceptibility with strain [3], or embedded fiber Bragg grating strain sensors for their change in refractive index with strain [4, 5].

There exist many methods for structural health monitoring, such as ultrasonic lamb waves or X-rays and acoustic emission. Ultrasonic lamb waves propagate in solids, and depending on the thickness or material that they are incident on, they interact with that medium differently. Structural health monitoring techniques use lamb waves to reflect particular features such as fatigue cracks, voids, and debonding in the sample, which requires intensive effort to reconstruct the detectd signals reliably and efficiently [6]. Acoustic emission is more for diagnosis after failure for determining the modes of failure and entails translating acoustic emissions upon failure into specific modes of failure, as first established by [7]. However, decoupling noise from the actual signal and determing the number of sensors necessary to detect the sound waves has made acoustic emission an open area of research. Because these methods are costly and time-consuming [8], there is a search for more effective but less intensive method of structural health monitoring. Other methods involve incorporating external sensors within the structure, but often at the cost of mechanical properties as this introduces additional modes of failure, such as interface debonding or pullout. Some SHM techniques may also be used as NDE techniques for diagnosing mechanical damage in a structure, such as using external acoustic emission. However, NDE techqniques may also be time intensive, such as tomographic imaging techniques, which allows for reconstruction of damage in the sample by intensity and location but require a large the number of sensors to effectively cover the expanse of the sample [6].

1.2 An Overview of Carbon Nanotubes

Since carbon nanotubes were first discovered in 1991 [9], research of CNTs has resulted in various applications such as sensors and hydrogen storage [10]. CNTs are allotropes of carbon with cylindrical structure and can be thought of as graphene sheets wrapped in a cylinder shape. Depending on the orientation and configuration of wrapping, various chiralities of CNTs are possible, usually indicated with *(n, m)* indices. Depending on its chirality, the CNT may have metallic or semiconducting electrical conductance. Carbon nanotubes are usually described as single-walled (SWNT) or multi-walled (MWNT), which indicates how many layers of cylinders exist in a cocentric configuration, as shown in Fig. 2.

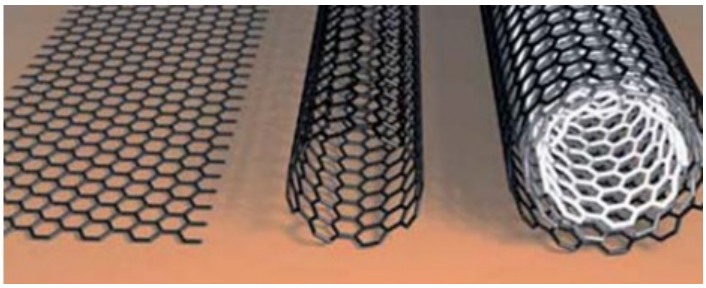

Figure 2: Ideal schematic representations of graphene sheet, SWNT and MWNT [1].

Synthesis of CNTs usually occurs by laser ablation of carbon rods, which consists of removing material from a surface via laser beam; direct current arc-discharge between electrodes, which involves applying a high voltage across graphitic electrodes to break down and deposit the carbon atoms; or chemical vapor deposition (CVD) [10]. This investigation utilizes CVD as the primary method of CNT synthesis. CVD is the process of breaking down gases at high temperatures into reactive species that deposit on a catalyzed substrate. Typical catalysts for CNT synthesis are transition metals such as Co, Ni, Pt, and Fe. CVD is advantageous for easily achieving uniform deposits of varying stoichiometry [11] and longer CNTs but often result in tubes with more defects than alternative methods of synthesis [1].

Though the entire mechanism of how the CNTs form is not fully understood, several theories exist. The most accepted model is the vapor-solid-solid model first proposed by Wagner and Ellis, which postulates that decomposed hydrocarbon gases precipitate on the surface of the catalyst and diffuses into the catalyst at which the CNT nucleates and grows from the edges of the catalyst particle. Two main models have been developed to describe how the CNT grows during synthesis: tip-growth and base-growth, as shown in Fig. 3. Tip growth involves the CNT lifting the catalyst particle and nucleating below whereas base-growth proposes that the catalyst particle remains on the substrate as the CNT grows above it [1]. Whether one mechanism

is preferred than the other is dependent on the catalyst and substrate system used, such as catalyst particle size [12]. Both growth mechanisms have been observed experimentally and computationally [1].

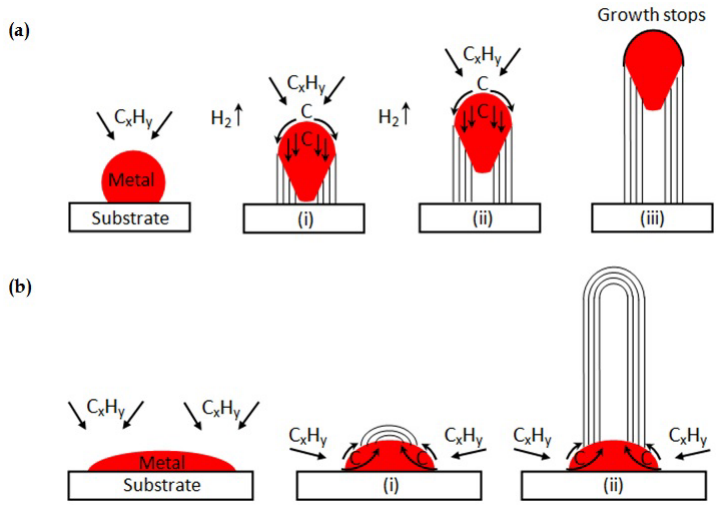

Figure 3: Accepted models for mechanisms of CNT growth a) tip-growth and b) base-growth [13]

The kinetics of the decomposition of the hydrocarbon gases have also been modeled [10, 14]. It is mostly accepted that ethylene first decomposes into acetylene. One kinetic pathway is the acetylene reacts with a hydrogen radical to form a vinyl radical and elemental carbon, which forms the CNTs. Several other pathways exist for the breakdown of acetylene into elemental carbon [10]. Other factors such as temperature and flow rate have been investigated to determine its effect on the synthesis of CNTs and amorphous carbon. Differences in synthesis of CNTs affect the mechanical and electrical properties, and thus impacts the behavior of the CNT as a mechanical damage sensor.

The property of CNTs most relevant to this investigation is the electrical conductivity of CNTs. The conductivity of CNTs may be calculated based on first principles basis in calculating the eigenstates of the Hamiltonian operator for the potential of a single electron in the potential of all the carbon atoms using the LCAO or tight-binding method. This involves first deriving the dispersion relation between energy eigenstats and the wavevector k. A plot of these resulting energy states in the band structure of graphene constrained to periodic conditions is shown in Fig. 4.

Fig. 4 is plotted as a function of energy and k-space. What is most notable about this plot is the periodic degeneracy of energy eigenstates between the conduction band and valence band that meet at a point that arises from the symmetry of the graphene lattice. That is, at select points along the graphene sheet are particular places where the conduction band and valance band meet. At these special points, charge carriers

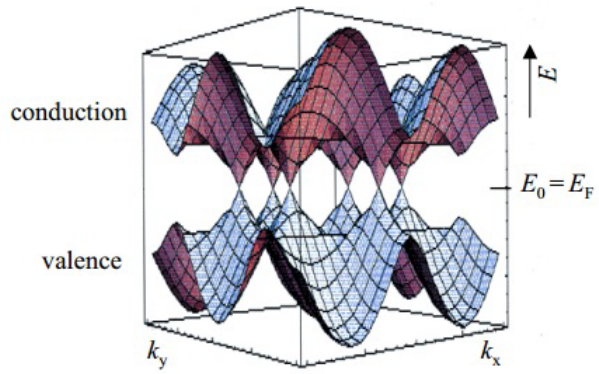

Figure 4: Electronic band structure of graphene, as derived from first principles calculation [15].

from the valence may cross into the conduction band easily at near zero effective mass, and conduct. The presence of defects or strain will physically bends this electronic band structure and alter the conductivity of the graphene sheet, making it a nanoscale sensitive material [15]. A carbon nanotube essentially may be abstracted as a graphene sheet wrapped in a cylindrical geometry. Each carbon atom is bonded to three other carbon atoms, with the fourth valence electron forming delocalized π-bands [16]. Depending on the how the graphene sheet is wrapped, various configurations and conducting properties of SWNT are possible. SWNT are categorized as either armchair, chiral, or zigzag, representative of how the graphene sheet wraps around. Fig. 5 presents the three major configurations of SWNTs, illustrating the various ways a sheet of graphene may wrap around itself. Depending on the SWNT configuration, the CNT may conduct like a semiconductor or metal.

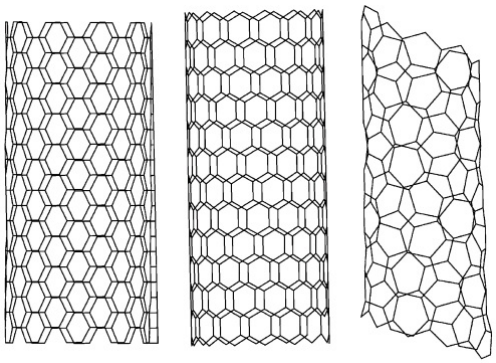

Figure 5: SWNT configurations: armchair(10,10) (left), zigzag(14,0) (middle) and chrial(7,3) (right) [17].

Armchair SWNTs are always metallic, zigzag SWNTs may be semiconducting or metallic and of all the chiral vectors possible, one-third are metallic and the remainig two-thirds are semiconducting [16].

Depending on growth conditions, CNTs of a wide variety of conductive properties may be grown. The electrical properties of MWNTs are more complex, and must take into account the interactions between concentric CNTs. Although coupling between concentric SWNTs in MWNTs occurs, it has been found that current primarily flows through the outer most nanotube [16]. The salient idea is that the conductivity of CNTs may be understood from first principles understanding of electronic band structure and may be manipulated through either the presence of defects or strain.

1.3 An Overview of Structural Health Monitoring in CNT Reinforced Composites

With composites being increasingly incorporated into aerospace structures, the desire to monitor or diagnose mechanical damage or damage accumulation has spurred many studies on how to best incorporate CNTs in the overall structure. Composites reinforced with carbon nanotubes (CNT), however, present a unique opportunity to monitor the structural integrity non-invasively. Unlike other methods of structural health monitoring, CNTs actually improve the mechanical integrity of the specimen. CNTs are exceptionally stiff and strong, up to 1 TPa and 63 GPa respectively [8], as well as electrically conductive for their size, up to several thousand Siemens per square centimeter for colossal carbon tubes [18] and hundreds of Siemens per square meter for CNTs [19]. Comparatively, CNTs are 100 times stronger than steel and can have metallic conduction 100 times more than copper over micron distances [1]. Moreover, due to their nano dimensions, the sensitivity of CNTs as damage sensors holds much promise. Although such properties have not fully translated to larger structure, CNTs have been shown to markedly improve mechanical properties, such as stiffness and toughness, in composite structures [20].

The conductivity of CNTs allow for the opportunity to simultaneously monitor the mechanical stresses sustained during operation. Damage to or around CNTs typically increases their resistance. Typical figures range from about 5% to up to 100% change in resistance correlated to around 1-3% strain or 1000-3000 micron strain, depending on how the CNTs are arranged, manufactured, into which composite matrix, and how the samples are mechanically deformed [21]. Various studies have shown that the percolating CNTs can be used to monitor a variety of structures, such as joints [22] and 3D composite structures [23]. It has also been shown that incorporation of CNTs into structures are capable of reflecting accumulation of mechanical damage under cyclic loading [22, 24] and sustain mechanical damage when impacted [25] with glass/epoxy composites with percolating CNT networks. Furthermore, CNTs as damage sensors have been shown to reflect various modes of failure, such as delamination using a thread of CNTs [26] and fatigue

through measurement of residual resistances, which manifested near the location of failure [24]. Thus, it is possible to monitor the stress and damage history of composites with CNTs using changes in a sample's electrical resistivity.

Several computational investigations on the electrical properties of CNTs in various matrix systems have also been conducted. Although many models simplify the complex mechanical interactions between CNTs and the surrounding matrix, they nevertheless show possible mechanisms through which the CNT network may be mechanically disrupted, such as matrix cracking [27]. Other models have demonstrated analytically the link between mechanical damage and changes in electrical resistance, which have shown good agreement with simulated models proposed thus far, such as with fiber breakage in CFRP composites using the shear-lag model [28]. Furthermore, it has been shown that the ratio of resistance change for uniform and unidirectional fibers for the longitudinal and transverse directions along the surface are idential and diverge for other geometrical configurations of the fibers, and both follow a general exponential relation based off of Weibull fracture [29]. Another investigation from [30] demonstrated possible mechanisms the CNT network is able to connect and deform with analytical and experimental methods. Fig. 6 shows an example of a resistance change with mechanical deformation for a simulated composite. Thus, analytically, CNTs demonstrate promise in localizing and correlating with the amount of mechanical damage.

There have additionally been many studies on CNTs or carbon fibers (CF) as sensors in many matrix systems, such as cement in various configurations [21, 31–34], on glass fibers [35–38], and in silicone rubber [39], that have achieved similar successes with carbon nanotubes as sensors for mechanical deformation and damage as with composite structures. However, structural health monitoring with CNTs in composite structures is still in early developmental stages. Several investigations that demonstrate the use of CNTs as structural health monitoring tools may be found in [40]. Thus, the focus of this investigation is non-destructive evaluation (NDE) of CNT reinforced composite structures towards the eventual implementation of such structures as part of the existing tools used in structural health monitoring.

The mechanisms through which CNTs or CFs are used to detect mechanical damage are twofold. First is the CNTs inherent piezoimpedence, a combination of its piezoresistance, piezocapacitance, and piezoinductance. That is, a mechanical deformation of the CNTs themselves causes a change in its electrical properties, such as resistance or capacitance. For example, loosely wound carbon fibers, which are composed of strung together CNTs, have greater capacitance as the gap between CNTs is larger [26]. Piezoresistivity is a property of the material itself and involves the physical deformation of the material's electronic band structure. Such changes in the CNTs have been investigated experimentally, such as [39,41], and analytically, in [42–44].

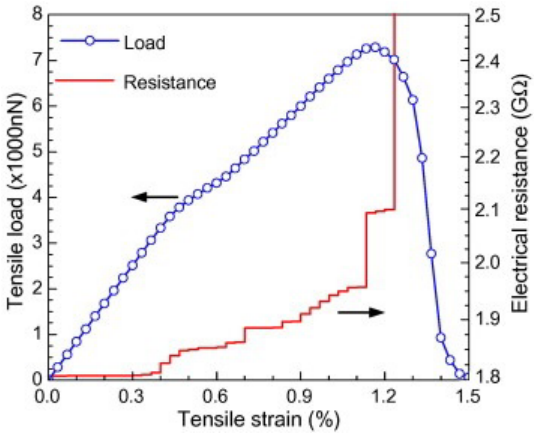

Figure 6: An example of modeling the variation of tensile load with electrical resistance for a [0°/90°/90°/0°] glass-fiber composite with embedded CNT network [27].

This piezoresistivity is a secondary mechanism to mechanical damage detection. Piezoresistivity inherent to the CNT itself is limited for very small strains, on the order of 0.5%, and deformations within this regime are typically reversible [45]. In most instances, at loadings above the percolation threshold and higher strains, the array and geometry of the CNTs dominates the measured electrical response, as damage accumulates. Typically, electrical resistance increases in tension as the CNTs or CFs are pulled and lose contact with one another and decreases in compression for opposite reasons [46]. This behavior has been experimentally observed [47, 48].

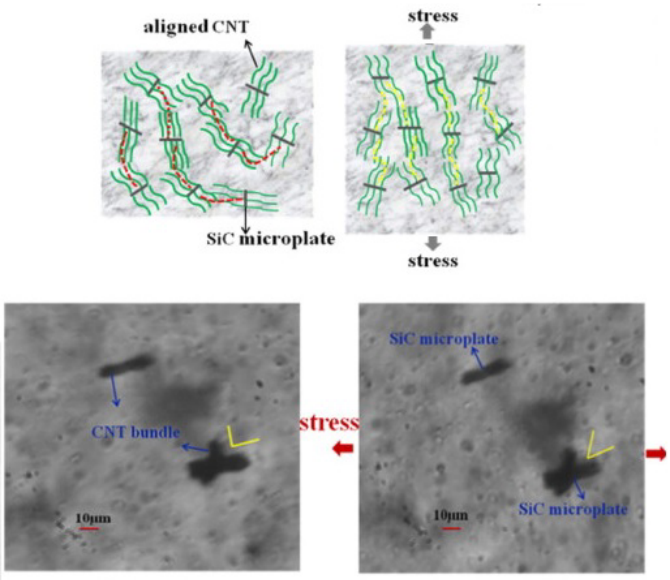

Figure 7: An example of how plastic deformation at 5% strain could affect local CNT network morphology and thus electrical resistance for CNTs grown vertically on SiC microplates(adapted from [47])

As Fig. 7 illustrates, plastic deformation could cause local deformations in the CNT network and CNTs themselves, and thus changes in local electrical resistance. For other CNT embedded composite constructions, it is also possible that fibers may delaminate from the matrix or that the matrix fractures, causing an increase in electrical resistance. Additionally, at the microscale level, small perturbations in the spacing between CNTs would also disrupt the possible tunneling that can occur [27]. It has been shown by [40] that the maximum amount of tunneling distance between CNTs in a polymer or ceramic matrix is about 1.8 nm, indicating that strains that deform the CNT network greater than this could indicate damage accumulation with large changes in measured electrical resistance. It is also expected that the geometry of the inclusions or CNTs also affects the degree of percolation and interaction between the CNT and the matrix. For instance, longer CNT fibers could entangle more and detangle less with mechanical strain in constrast with shorter CNT fibers. Another example was demonstrated by [30], in which adjacent CNTs were abstracted to have tunneling directly between CNT ends or between overlapping CNT regions for making conductive pathways in the sample, as depicted in Fig. 8, and demonstrated to be a possible mechanism for the damage acculumation of CNTs. The extent of dispersion, percolation, and arrangement, therefore, contribute significantly to the damage sensing abilities of CNTs. Thus, the overall measured electrical resistance of at the macroscale may be a confluence or statistical average of all such microscale effects.

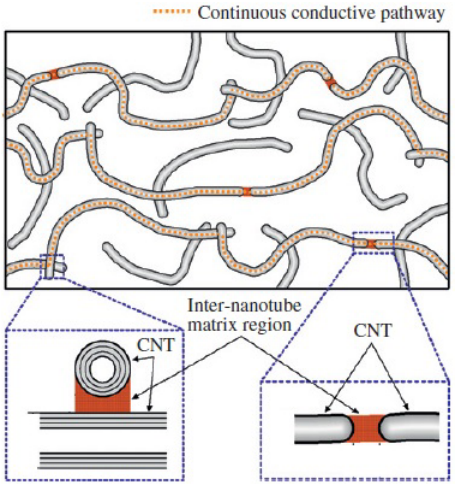

Figure 8: Proposed configurations for how a percolating CNT network forms connected conductive pathways through either between overlapping CNT regions or between CNT ends (adapted from [30]).

There exists two main methods of incorporating carbon nanotubes into a specimen, as carbon fiber [26,49] or dispersed throughout the matrix material as short CNTs such as [33]. Given the vast number of methods of synthesizes and dispersing CNTs in a matrix material, the full optimization of structural health monitoring

using CNTs remains incomplete.

1.4 Objectives

Current research into structural health monitoring has included various matrix materials, including aligned CNTs as a damage or strain sensing network. The focus of this study will be non-destructive evaluation towards structural health monitoring with aligned CNT reinforced composite structures. Many other investigations focus on the piezoresistivity of CNTs or carbon fibers (CF) in particular geometries as a strain, rather than damage, sensor [36–38, 50]. Many experimental investigations have looked at specific constructions with other materials such as glass fibers and arrangements of CNTs in a particular matrix, and most numerical investigations look at interactions between CNTs, such as tunneling, and so are not as accessible experimentally. This investigation will build upon composite architectures of aligned CNTs that have been shown to have enhanced mechanical strength and toughness [51], to take advantage of the multifunctional properties of the aligned CNT networks done in NECSTlab at MIT, evaluate the damage sensing capabilities of CNTs in the architecture and methods used previously, and provide insightful data for the industrial application and usage of aligned CNTs in aerospace composites. Two major architectures, the nanostitch and fuzzy fiber constructions, along with testing CNTs as a material strain gauge are tested and evaluated, comparing the sensitivity of electrical resistance with changes in mechanical load and history.

1.5 Motivations

Although there has been substantial research into CNTs as mechanical damage or strain sensors. This investigation uses the CNT synthesis methods outlined in [52], which provides the basis of the recipes used for growing CNTs and the methodology for obtaining aligned CNTs of controllable morphology. Nanostitch and fuzzy fiber CNTs are the two major network architectures used in this investigation. The basic geometric configurations are shown in Fig. 9.

These two particular constructions are investigated because of the advantageous mechanical reinforcement they lend to the composite structure. The nanostitch architecture borrows from the idea of Z-pinning, in which reinforcing fibers are added to the composite structure to reinforce the interlaminar regions (i.e. z-direction) where the composite is often the weakest. However, such fibers are added at the cost of losing intralaminar mechanical integrity due to the added material interface and damage introduced. Instead of adding macroscopic fibers that also mechanically weaken the composite, nanostitching is the idea of adding CNTs as the pinning agents. Due to the minimal amount of CNTs for refinforcement, nanostitching presents

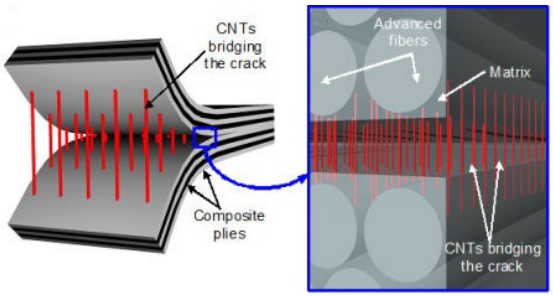

(a) Nanostitch architecture in which CNTs reinforce against crack propagation at the interface [53]

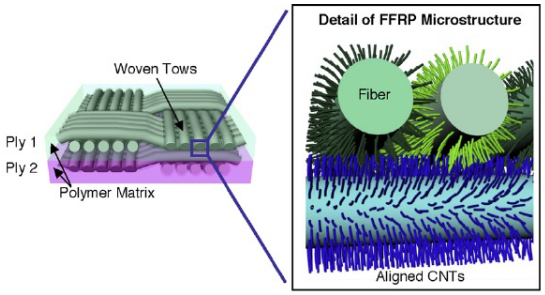

(b) Fuzzy fiber architecture in which CNTs are grown radially around a ceramic woven fabric [51]

Figure 9: CNT network architectures investigated

a method for minimal added cost for mechanical reinforcement, without trade off from added weight or introducing other mechanisms for the composite to fail. The mechanism of toughening the interlaminar layers to crack propagation is primarily pull-out of the CNTs. Analytically modeling various pull-out mechanisms for MWNTs, [54] found that CNT nanostitch reinforcement was significantly more effective in comparison to standard methods of interlaminar reinforcement.

The fuzzy fiber construction considers interlaminar and intralaminar reinforcement. Because CNTs are grown radially around the woven substrate, CNTs are able to penetrate within and across each layer, providing additional mechanical reinforcement. Fuzzy fiber reinforced plastic (FFRP) composites have been shown to improve interlaminar shear strength by 69% to around 34 MPa [55], tension bearing stiffness by 19% to 30 MPa, and interlaminar fracture toughness by up to 76% in steady-state to 3.74 kJ/m^2 when compared to the baseline without CNT reinforcement for the geometry used, which illustrates that such a CNT network offsets composite failure [51]. Additionally, the FFRP structure has shown promise as one appropriate for structural health monitoring in impact damaging tests, as demonstrated in [56], using resistive-based measurements and tomographic imaging to spatially represent damage. Similar success has been attained using thermographic damage detection to spatially resolve the location of damage using resistive heating in local areas of damage [57].

Given that such CNT network architectures are mechanically reinforcing in composites, the objective of this investigation is to evaluate the extent that the CNT networks may also serve as sensors for mechanical damage and failure in the nanostitch and FFRP CNT hierarchical architectures developed.

2 Experimental Approach

Three different specimens were prepared to investigate the NDE capabilities of composites reinforced with carbon nanotubes: carbon fiber reinforced epoxy plates using typical aerospace industry materials produced by Hexcel Corporation, pre-fabricated and industrially purchased DragonPlate plates, and FFRP composites. Each specimen underwent open-hole tensile tests. A hole is drilled into each sample to serve as an a stress concentration area to control the location and manner of sample failure. It is well known in continuum mechanics that a circular defect in a structure results in a stress concentration factor that triples the applied stress around the immediate area surrounding the hole for isotropic materials, and has a similar effect for heterogeneous materials such as the composites tested. Introducing such a feature controls the failure mechanism and strain at which the samples fail, and eliminates part of the variability due to manufacturing. The testing matrix is presented in Table 1 below. A full description of each sample may be found in Appendix A. Specimen type and number were limited by manufacturing and time constraints. Hexcel samples were not nanostitched due to constraints in available CNTs.

Table 1: Test matrix and sample types with notation used; HP = Hexcel with CNT Patch, HC = Hexcel control, FFRP = Fuzzy Fiber Reinforced Plastic, DP = DragonPlate with CNT Patch, DC = DragonPlate control

Notation	Type	Probe Configuration	Samples Tested
DP	DragonPlate w/ CNT Patch	vertical	5
		horizontal	5
DC	DragonPlate, control	vertical	2
		horizontal	2
HP	Hexcel w/ CNT Patch	grid	5
HC	Hexcel, control	grid	2
		vertical	1
		horizontal	1
FFRP	Fuzzy Fiber Reinforced Plastic	grid	5

DragonPlate samples are quasi-isotropic carbon fiber plates purchased industrially. Hexcel samples are carbon fiber prepreg with CNTs on the surface of the two outermost plies, in order to produce a reliable electrical contact to the carbon fibers, due to limited materials. FFRP samples are laminates in which CNTs are grown radially from a woven substrate and infused with epoxy resin. Each type of sample is constructed with different architectures of the CNT networks and varying degrees of integration with the rest of the structure. DragonPlate samples have no CNTs incorporated in the sample but have unidirectionally knocked down CNT patches adhered to the surface like a strain gauage. Hexcel samples have either a CNT patch or not, and all samples have unidirectional CNTs stitched at each of the interfaces. FFRP samples have CNTs

fully integrated in the samples.

2.1 Sample Manufacturing

In order to evaluate the capabilities of CNTs as structural health sensors, all samples were tested under open-hole tension. Sample preparation was twofold- manufacturing and circuit preparation for simultaneous measurement of electrical resistance with increasing mechanical strain. Samples with CNTs incorporated within the specimen had electrode probe configurations in a grid in order to measure the through thickness resistance; samples with no internal CNTs had knocked-down CNTs adhered to the surface with electrode probes configured horizontal and vertical to the tensile direction, as explained later in this section. These electrode configurations were both tailored to the location of the CNTs in the sample. Sample preparation is presented in the order of manufacturing, electroding, cutting to testing dimensions, and testing parameters used.

The first kind of sample tested was carbon fiber reinforced polymer laminates made from unidirectional Hexcel 8552/AS4 prepreg tape, which is essentially carbon fibers preimpregnated with partially cured (b-staged) epoxy. More information on this material may be found at [58]. Each sample had $[(0/90/\pm 45)_2]_{s16}$ lay up, which translates to two repeated layers of 0, 90, +45, and -45 degree fiber orientations laid out symmetrically about the x-y plane such that 16 layers in total are laminated and cured. In a 16 layer composite, the outer surfaces were adhered to unidirectionally knocked-down CNT patches; in future work, nanostitching would be introduced before the curing stage, and involves growth of forests and transfer of forests onto the prepreg material. Growths were on the order of 100 - 120 microns on silicon wafer substrates with deposited catalyst. After growth, the forest was transfered to the prepreg in such a way to preserved the aligned nature of CNT synthesis and cured, based on [59]. An example of such a transfer is shown in Fig. 10. The prepeg was prepared according to the procedures outline in TELAC manufacturing guide for prepreg, as available to NECST lab members. Essentially, the prepreg material is sandwiched between metal plates and several layers of non-stick materials under vacuum to ensure even distribution of heat and epoxy during the curing stage. All samples are then cured under the cure according to the temperature cycle for monolithic components as specified by [58]. The final samples consisted of carbon fiber plastic reinforced plates cured such that in between the outer layers are aligned CNTs. Ten samples in total were prepared, five with CNT patches and five without as controls. A summary of the samples may be found in Table 1.

Samples with pre-frabricated plates were quasi-iso graphite epoxy (DragonPlate FDPLHP04S1212) of the final desired thickness (3.175 mm) were purchased industrially from [60]. Additional information on the

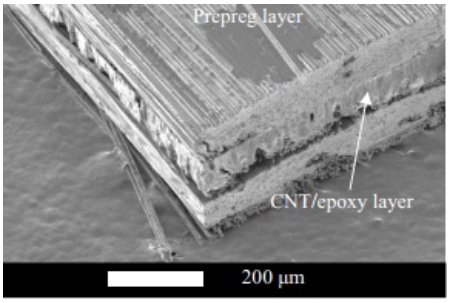

(a) SEM image of example of single layer nanostitch layer

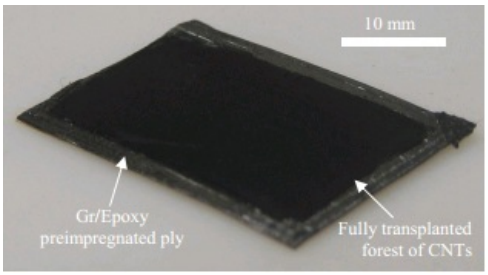

(b) Nanostitch sample without top prepreg layer

Figure 10: Example sample of nanostitching (adapted from [59])

mechanical properties of DragonPlate may be found at [60]. The DragonPlate material is a carbon fiber composite used currently in industrial and aerospace applications. Fourteen total samples were prepared. Ten samples had CNT patches and the remaining four had no CNT patch adhered.

FFRP composite samples were made using CVD synthesized CNTs and West Systems (105 resin, 206 hardener) epoxy on 391 W-2 alumina cloth from Cotronics. Alumina cloth was dipped in 50 mM iron nitrate with isopropanol solution to react as catalyst. CNTs were synthesized on the alumina substrate based on the procedures outlined in [52] and [51], but had 350 standard cubic centimeters per meter (sccm) of ethylene flowing, with 2070 sccm hydrogen and 1040 sccm hydrogen as appropriate in the recipe used. Various times were used to achieve different percent weight gains, and thus CNT lengths. Five samples in total were prepared, each centered around 1.0, 2.0, 3.0, or 4.0 wt% gain in CNTs. Plies were grown such that CNTs were at least 10 microns long to allow for sufficient percolation of CNTS in the epoxy matrix. Further information is listed in Appendix B. Table 2 provides a summary and relevant notation for the FFRP and other samples. Full descriptions of the FFRP and other samples may be found in Appendix A. Additional information on the growing conditions of the CNTs may be found in Appendix B. Laminates were manufactured using hand lay-up and consisted of 6 plies centered around the appropriate weight gain in CNTs. The manufacturing process involves alternating between pouring resin and laying up the plies manually, such that bubbles are minimized and the epoxy is given sufficient time to wick through the ply. The laminates were sandwiched between two metal plates that were placed under vacuum and compressive clamping in order to achieve the desired thickness and thus volume fraction desired. Spacers of the desired thickness were placed betwen the metal plates. The metal plates are intended to distribute the clamping force uniformly and encourage air voids to squeeze out of the ply. Once a sample was clamped down, the vacuum was removed and the sample was allowed to cure at room temperature for at least 24 hrs. All

materials were encased in vacuum bagging and other additional non-stick layers as needed in order to be able to extract the cured sample.

2.2 Electroding Samples

After the appropriate curing conditions, all samples were then prepared with electrodes, in order to allow for simultaneous measurement of resistance and mechanical deformation. Hexcel and DragonPlate samples with knocked down CNT patches of 80 mm x 30 mm dimensions were co-cured for an additional hour at 121°C using surfacing film (Tencate TC235-1SF) as adhesive. The CNTs were knocked down such that they aligned parallel with the direction of tensile load. The knocked down CNTs were thinner than the film adhesive, and so were not in contact with the sample. For the control samples, silver paint was applied to a layer of adhesive so that the paint was not in direct contact with the sample. All samples had several layers of silver paint (Ted Pella 16045 from [61]) stenciled and baked at 151°C onto either the sample or the CNT patch, where relevant. Flexible printed circuit boards and further connections were used to build the remainder of the circuit; the flex circuits were wrapped around the sample and adhered using 3M VHB tape. All electronic components attached to the sample were chosen to minimize mechanical contributions to the load curve. Resistance contributions that are not the sample itself included the 2m Samtec FFSD-06-D-39.00-01-N-RW cables between the sample and relay, solder, and flex circuit, with the largest contribution being the cables at around 0.5 Ohms/m. The total resistance measured from the intruments measured was approximately 0.8 Ohms. These resistances were found to be fairly consistent across samples and tests.

Three different configurations were used with the silver paint electrodes, depending on the sample and where the CNTs were placed in or on the sample. DragonPlate and control samples were configured with either horizontal (H) or vertical (V) silver paint, in which the silver paint extended perpendicular or parallel to the tensile direction respectively. Remaining samples were grid (G) configured, in which one side of the sample had the horizontal configuration and the other side had vertical configuration. Each configuration had effectively 24 lines silver paint probes, each of 0.5mm thickness and spaced 0.5mm apart with 1.5mm space at the edges of the samples. Measurements were taken between pairs of adjacent probes across consecutive sections of surface the sample and across the width of the sample as well for the H and V configurations; measurements where taken through the thickness of the sample in locations away and near the hole for the G configurations. Fig. 11 and Fig. 12a provides a schematic for each configuration and the corresponding locations on the sample of resistance measurements; Fig. 13 provides dimensions of the the probes and spacing of the probes used. For clarity (see Fig. 11), in the H and V configurations, Probes 1-5 correlate

with 'far field 1', Probes 10-15 with 'near hole', and Probes 19-23 with 'far field 2' measurements; Probe 24 corresponds with the total resistance measured across the the entire sample. In the grid configuration, Probes 1, 6, 11, 16, 41, 46, 51, 56 are 'far field' and Probes 23, 28, 33, 38, 24, 29, 34, 39 are 'near hole'. Measurements of resistances are made between silver paint probes.

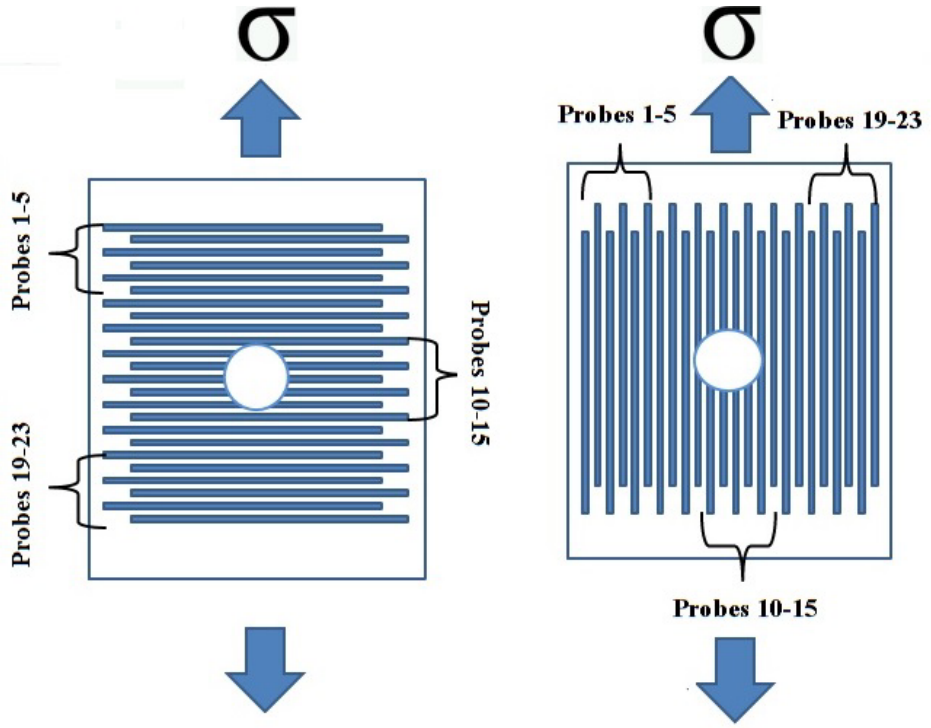

Figure 11: Schematic of horizontal (H) and vertical (V) silver paint configurations used for samples with respect to tensile direction, as specified in Table 2; resistance measurements occur between silver paint probes (blue); probe labeling is the adopted convention to describe where the measurement was taken.

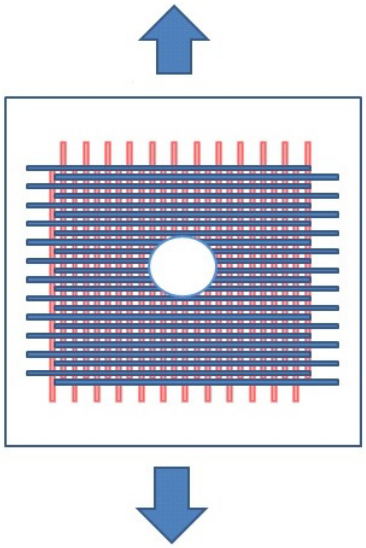

(a) Schematic of grid (G) silver paint configurations for measuring through-thickness electrical resistance; one side of the sample has H configuration and the other has V configuration for effective grid configuration.

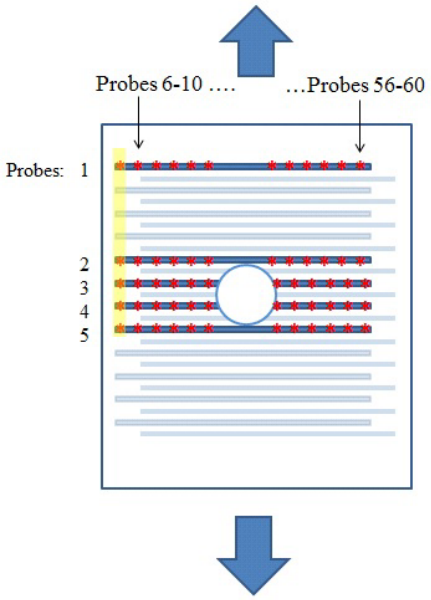

(b) Schematic of grid (G) silver paint configurations, highlighting the locations at which resistance measurements were taken (marked with red asterisk).

Figure 12: Schematic of grid (G) silver paint configurations.

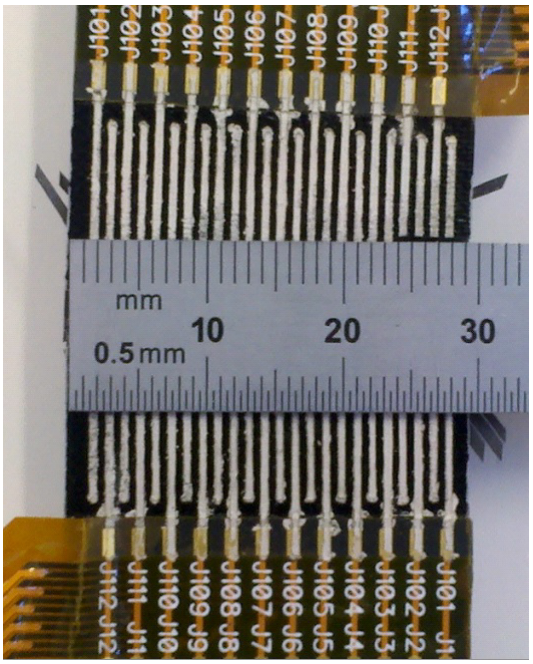

Figure 13: Close up and dimensions of the the silver paint used as eletrical probes for resistive measurements of all samples.

In order to extract the resistance of the sample, the sample was connected in ciruit in series with a resistor and connected to a solid-state relay that measured the resistance across each location at 1 Hz frequency. Fig. 14 shows the schematic used; relays and other measurement instruments are not shown. Using Ohm's law, the current flowing through the system is extracted from the measured voltage V_- and known resistance. The voltage V_+ is approximated to be the voltage source. From this, the resistance of the CNT can be extracted.

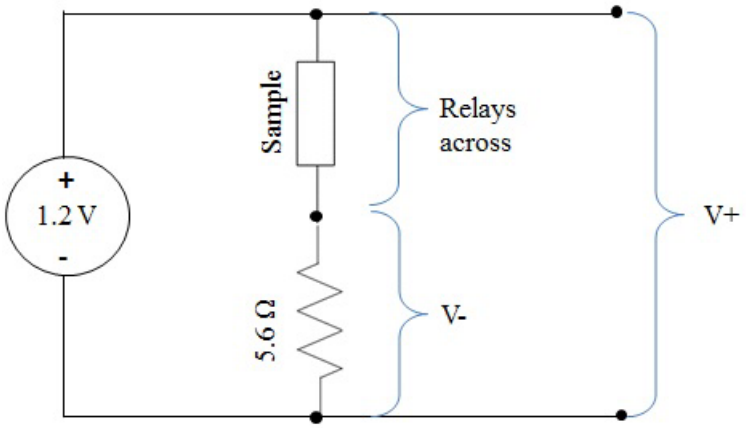

Figure 14: Schematic of circuit used to extract resistances of samples tested; relays and other solid-state instruments are not shown

Resistances not part of the sample of note include the electrical components, of which the cable contributed the most at approximately 0.5 Ohms/m with total system resistance of 0.8 Ohms. However, these resistance contributions were constant and confirmed as such before each test conducted. The most variable resistance that would affect the data would be that of the silver paint, particularly as it deforms. Because of this, controls with only the silver paint were manufactured in order to understand the extent that silver paint probe failure without the presence of CNTs occurs.

2.3 Sample Testing Parameters

Samples with CNT-patches were prepared to be 252 mm long by 30 mm wide and ranged in thickness between 2.0 and 3.3 mm. Due to manufacturing constraints in growth consistency, FFRP samples were prepared to be 200 mm long by 30 mm wide and ranged between 2.1 and 3.1 mm in thickness. A full description of dimensions per sample is listed in Appendix A. All samples were cut to dimensions using a diamond saw and had a 5 mm hole in diameter drilled with a carbide brad point bit and reamed with a 5 mm diameter carbide reamer to ensure that the hole would minimally disturb the surrounding material. All samples were

prepared in accordance to ASTM standards D5766/D5766M-11. All samples were sanded at the edges and taped to sand paper for better gripping during tensile tests. Figs. 15 and 16 show example samples during the open hole tensile tests, and the remaining failed specimens. Fig. 16 shows typical failed samples of each type of sample tested.

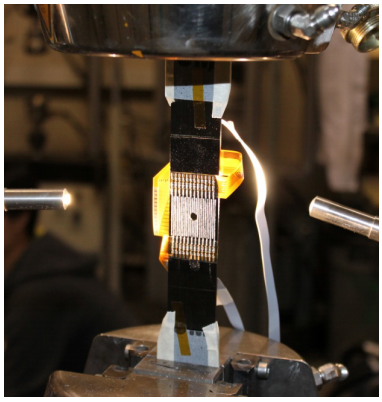

Figure 15: A sample during tensile testing

For testing, an Instron 1332 was used to pull the samples in tension until failure. Samples 1 through 10 had 2000 psi clamping pressure and remaining samples had 3000 psi clamping pressure, due to slippage problems for some samples. A 100 kN load cell was used with 0.25 mm/min strain rate. Data was collected at a frequency of 1 Hz for both the load and electrical resistance measurements at each location indicated.

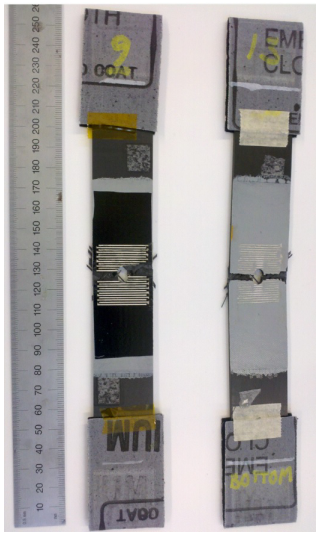

(a) Fractured DP9 (left) and DC3 (right)

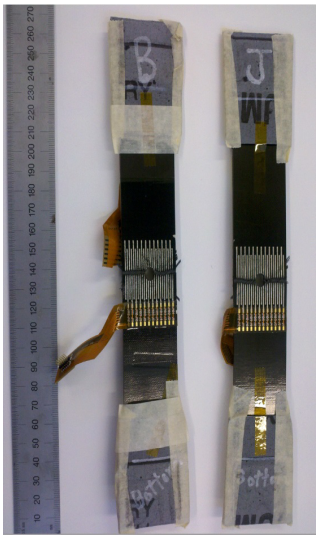

(b) Fractured HP2 (left) and HC3 (right)

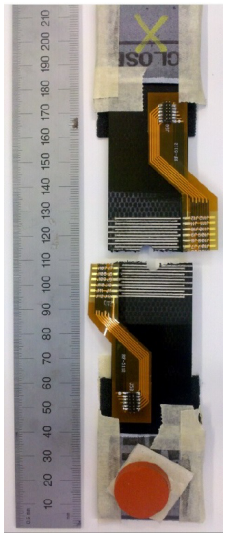

(c) Fractured FFRP3

Figure 16: Typical samples after failure

3 Results and Discussion

This section presents the results of the open-hole tensile tests according to the sample type and individually evaluates the capabilities of CNTs as structural health monitoring sensors as both an external strain gauge and incorporated method of mechanical reinforcement. As illustrated in Figs. 11 and 12, many sets of resistance measurements were taken across the sample. For the H and V configurations, a total of 24 measurements were made per second across the samples- 23 at consecutively adjacent positions across the sample and one across the width of the furthest spaced probes. For the G configuration, a total of 60 different resistance measurements occurred every second. Particular measurements correlating with specific locations on the samples are highlighted and labeled, and are referenced as so in the data analysis and figures.

3.1 Damage Sensing in Industrial DragonPlate samples

DragonPlate samples consisted of an industrially purchased quasi-isotropic graphite epoxy composite manufactured at the desired thickness of 3.175 mm. DragonPlate is a common industrially used aerospace composite material. The motivation for testing industrially made samples is for demonstration of the basic capabilities of the structural health monitoring capabilities of CNTs. As many new technologies must pass through several engineering and industrial criteria to be accepted as common technology, there is a large time of integration of such new technologies into the status quo. Thus, many of the newer developed architectures

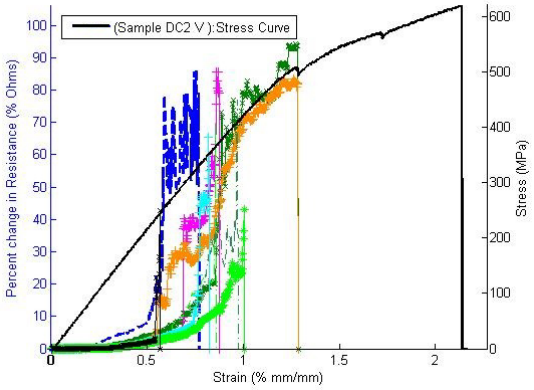

(a) Correlation of stress and changes in electrical resistance for all non-open circuit probes in control sample DC2 of the 24 probes, illustrating early probe failure; probes measuring open circuit are not shown.

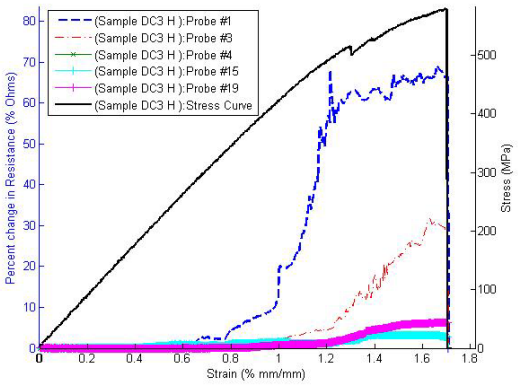

(b) Correlation of stress and changes in electrical resistance for the sets of probes that exhibited potential in health monitoring

Figure 17: Overlayed stress curve with measured resistance changes for representative DC control samples, with silver paint, adhesive, but no CNT patch.

of CNT composites, such as nanostitch and FFRP, would not enter the market as readily. However, the DP samples consider adding CNTs superficially, such as with a strain gauge patch on the surface.

Because these samples do not have CNTs integrated within the structure, DragonPlate (DP and DC) samples had knocked-down CNTs adhered to the surface as a strain gauge. Fourteen samples in total were DP; five were in horizontal (H) configuration, five in vertical (V) configuration and the remaining four made without the CNT patches as controls, divided evenly between the H and V configurations.

Of the control samples tested, a limited few exhibited the ability to monitor the health of a structure using silver paint probes alone. Fig. 17 illustrates that only a select few probes randomly scattered across the sample of the control samples successfully showed an ability to correlate with the loading of the curve. Each plot is labeled with the probes plotted in the format of '(Sample [SampleName] [probe configuration]: [probe])'; for instance '(Sample DP1 V): Probe #23' would correspond to the 23rd probe of sample DP1 in vertical configuration. the probes Probes that measured open circuit resistance values correlate with very large values of resistances, and so are not shown with respective plots. The second displayed sample had the most number of probes that did not prematurely fail or did not exhibit substantial noise. This suggests that although it is possible to use only silver paint on top of adhesive, it is unpredictable and unreliable with silver paint and adhesive alone. These plots demonstrate the variability of the probes made and potential false contributions to the change in resistance measured. All plots are overlay of strain (% mm/mm) with percent change in resistance (% Ohms) and stress (MPa).

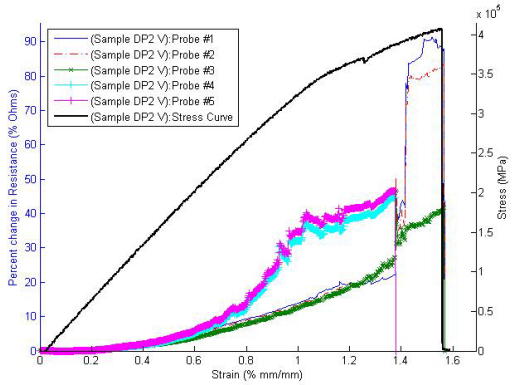

(a) Correlation of stress and changes in electrical resistance in far field 1

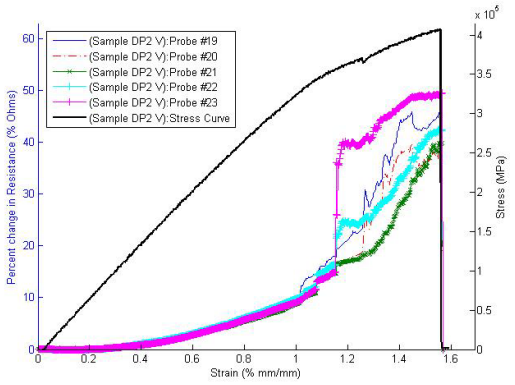

(b) Correlation of stress and changes in electrical resistance in opposite far field 2 from previous

Figure 18: Overlayed stress curve with measured changes in opposite far field electrical resistances of sample DP2 in V configuration

Fig. 17 establishes that structural health monitoring using the strain sensing capabilities of the silver paint and adhesive alone is insufficient for reliable structural health monitoring. The remainder of the section therefore focuses on samples with CNT patches adhered to the surface of DP samples. Fig. 18 illustrates a typical curve of the DP samples with vertical probe configuration. A fuller list of figures for each sample tested is located in Appendix C. Due to the volume of potential plots possible, a select number are highlighted for the particular features they illustrate. Because of the variability of manufacturing the probes and samples, some probes reached failure before the sample; thus the data for some probes terminate earlier than the failure strain of the sample. A full description of the failure loads and strain of each sample tested may be found in Appendix A.

The mechanical behavior of the DP samples consists of a linear range that suggests elasticity and a region of plastic deformation where the sample becomes more compliant until the point of failure, marked as a sudden drop in stress in the stress-strain curves. Several features of Fig. 18 are representative of other samples tested in similar configuration. For many DP samples, the typical strain at failure occurred around 1.5-2.0% elongation. The onset of greater compliance also occurred regularly within the DP sample set at approximately 1.0% strain, which indicates that any inconsistencies measured in the electrical resistance probes are mostly due to the manufacturing of the probes themselves than with the samples. Because of the large variation between the probes, even within the similar locations of the sample, determining an analytical relation of strain and change in electrical resistance would prove unfruitful. Nevertheless, several salient features of all DP samples were found that were indicative of the CNT patches as diagnostic tools

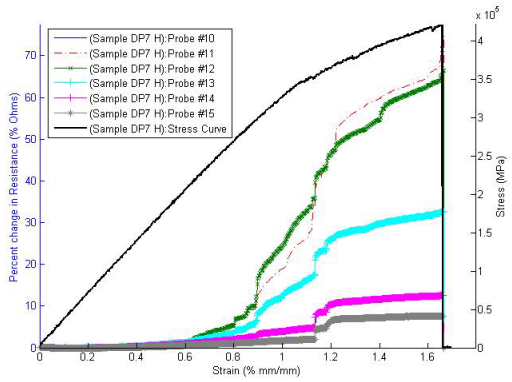

(a) Correlation of stress and changes in electrical resistance near the hole

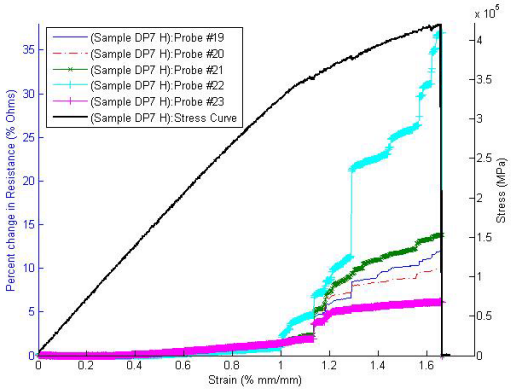

(b) Correlation of stress and changes in electrical resistance in opposite far field 2 from previous

Figure 19: Overlayed stress curve with measured changes in resistance opposite far field electrical resistances of sample DP7 in H configuration

for mechanical damage accumulation.

As seen in Fig. 18, particularly in Fig. 18b, there is a direct correlation between changes in the mechanical behavior of the sample and changes in electrical resistance. In the first linear regime, the change of electrical resistance remains below 1.0% Ohm change and is smooth and continuous. Upon reaching the second regime suggestive of damage (increased compliance), changes in resistance are sudden, incidating a correlation of mechanical accumulation beyond piezoresistivity of the CNT patch and the sample. For most of the DP samples, regardless of position of measured resistance, the maximum change in resistance measured jumped beyond 10% Ohm resistance change and continued to increase in sudden jumps once the sample entered the second regime of elongation. The final measured change in electrical resistance at time of failure varied between 30% and 120% Ohm change, and may be partially due to the variability of probes made (see Fig. 17 and discussion).

Similar behavior was seen with the horizontally configured DP samples. Fig. 19 illustrates similar small monotonic increases in the electrical resistance in the initial regime and then transitioning to more sudden and larger jumps in the change in resistance in the 'plastic' regime, or increased compliance in an inelastic region. Similar ranges and values of changes in electrical resistance were found with the H configuration. Plots for other DP samples showing similar behavior are included in Appendix C.

However, the generic shape between the H and V configurations of the DP samples were noticably different. The spikes in electrical resistance of the V configured samples often occurred in 20-40% Ohm intervals. Some of these jumps correlated with the onset of compliance and others before the failure of the

probe itself. In constrast, the spikes of the changes in electrical resistance for the H configured samples were more gradual, and occurred in smaller changes on the order of 5% Ohm change. Two possibilities may explain the difference in meausured change of electrical resistance. The first may be due the variability of probe manufacturing. Vertical configured samples were stenciled with silver paint before horiztonally configured samples, so it is possible that improved consistency of applying the silver paint also improved with the number of samples made.

In comparing the consistency of the change in electrical resistance in similar locations on the sample, as illustated with Fig. 18 and 19, the location of the resistances measured do not correlate. That is, measurements near the hole and far from the hole are consistently extremely varied between 10 and 100% resistance change at point of failure across the DP samples. This may be attributed to the fact that, because the CNT patches are not an integrated part of the structure, the strains it measures is limited to the efficacy of the adhesive to simultaneously transfer the strain of the sample to the CNT patch and minimally contribute to the meausured mechanical behavior of the sample. This indicates that although the CNT patch is able to detect points on the sample where mechanical deformation occurs, it is not possible to correlate that measurement with its proximity to a stress concentrator.

However, upon holistic evaluation of the DP samples, the consistency of this behavior between H configured samples versus V configured samples, suggests that the orientation of the CNTs patches with respect to the orientation of the probes influences the stability of the change in electrical resistance. As explained in Section 1.1, strains beyond the range of piezoresistivity causes deformations of the CNTs and the CNT network, and depending on the configurations of the CNTs, influences the conductive network for which charge carriers are able to flow, thus influencing the overall resistance of the sample. Because the CNT patches are unidirectionally knocked down CNTs, the major mechanism of CNT network deformation under tensile loading is the CNTs pulling apart, as illustrated in Fig. 20. As the CNTs pull apart, the effective conductive pathways for current to flow through decreases, and therefore resistance increases.

In the V configuration, the CNTs are parallel to the silver paint probes. It is possible that because the silver paint probes are in parallel to the knocked down CNTs, the measured resistances are more sensitive to local changes in resistance of a few CNTs as they are stretched and pull apart from each other. In contrast, because the H configured samples are perpendicular to the knocked-down CNTs, the H configured probes measure changes in resistance across the width of the CNT patch and so is less sensitive to local changes in CNT network deformation. Thus the resistance jumps in the H configured samples are smaller and more consistent between probe location. This suggests and reinforces the hypothesis that the arrangement and

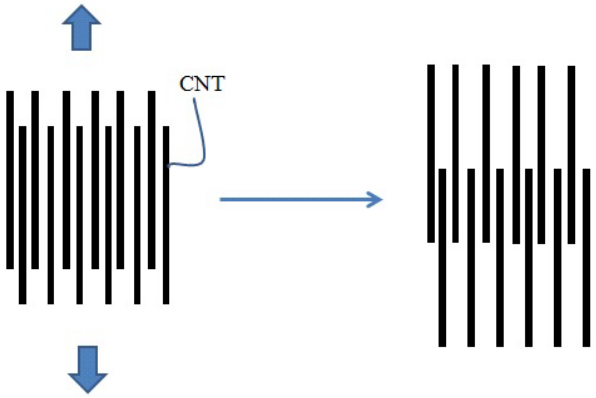

Figure 20: Proposed mechanism of CNT network deformation of CNT patches with respect to tensile direction adhered to DP samples; with increasing load, the CNTs, simplified to be like teeth on a comb, are pulled apart; in the actual sample, variation in the local CNT network topography is expected and so local changes in the CNT network topography would also vary.

topography of the CNT network has a large influence on the resistance measured. These results also suggest that for unidirectional CNTs, measuring the resistance perpendicular to the direction of the CNTs offers less noisy and more holistic understanding of the structural health of a part.

In most practical cases in industry, however, resistance measurements would be taken across the span of the structure instead of at particular spots on the structure, in order to save of time and cost. Fig. 21 shows typical curves for the total resistance measured across the DP samples from both the H and V configurations; total resistance measurements across the the span of the silver paint probes correlates with Probe 24, in the convention adopted. Plots from other samples and illustration of probe failure are in Appendix C.

As illustrated in Fig. 21 measuring the total resistance across the span of the sample is an effective way of tracking the mechanical lifetime of a structure using the CNT patch. All samples exhibited correlation between change in electrical resistance and changes in the mechanical behavior of the sample. There is also a clear demarcation between the two different regimes of the load curve. Fig. 21 also demonstrates that it possible to track the health of a structure regardless of the position of the stress concentration and regardless of the distance of the measured resistance with respect to the stress concentration.

Fig. 22 shows a typical cross section of the area surrounding the stress concentration and examples of failure such as delamination and fiber breakage. This demonstrates a physical manifestation of the mechanical damage inferred from the change in resistance curves.

Overall, CNT patches on DP industrially purchased samples were found to have promise as a diagnostic tool for structural health monitoring of composites. Although in these particular samples, it was not possible

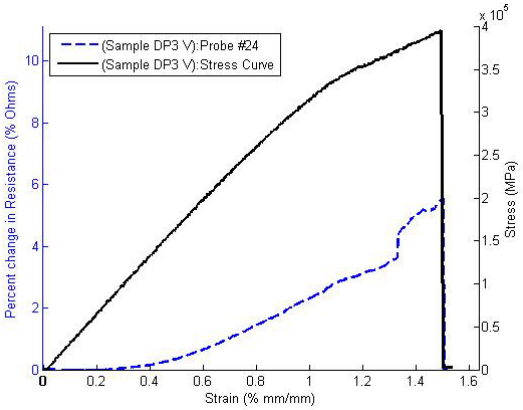

(a) Correlation of stress and total measured changes in electrical resistance for sample DP3

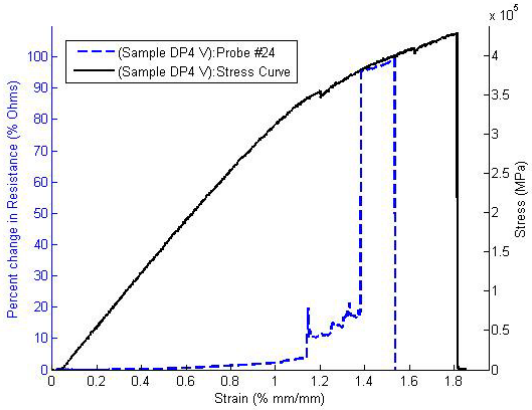

(b) Correlation of stress and total measured changes in electrical resistance for sample DP4

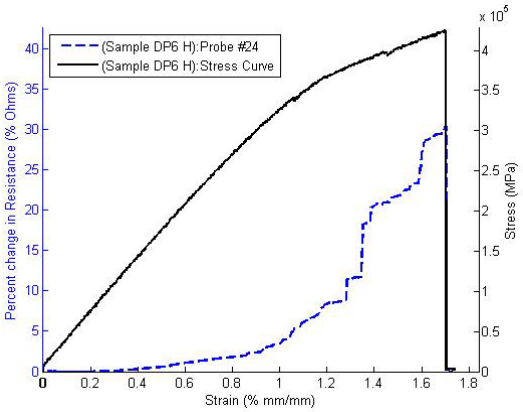

(c) Correlation of stress and total measured changes in electrical resistance for sample DP6

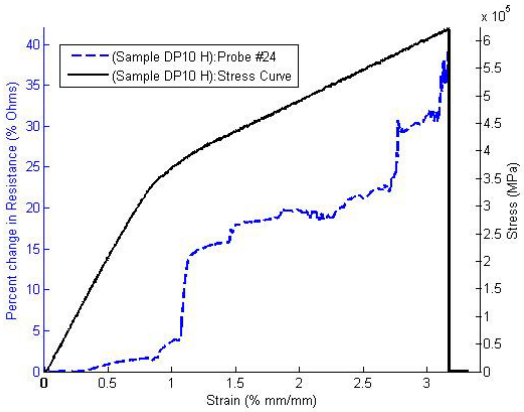

(d) Correlation of stress and total measured changes in electrical resistance for sample DP10

Figure 21: Overlayed stress curve with total measured resistance changes for DP samples in H and V configuration; total resistances measured correlates with Probe 24 in adopted conventions

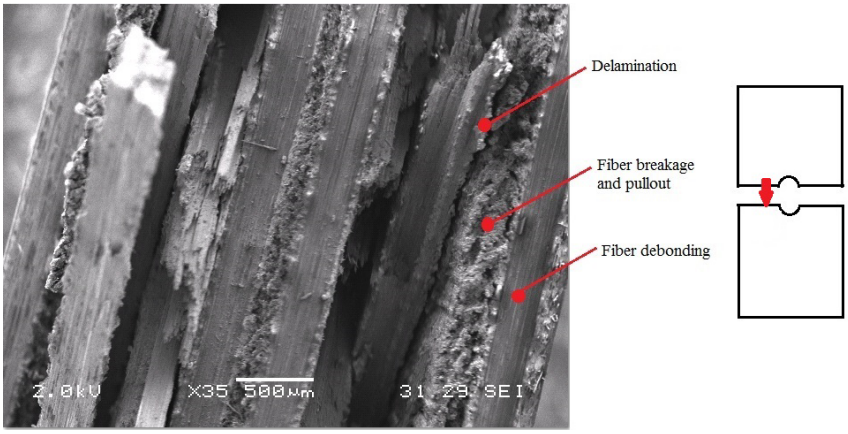

Figure 22: SEM of cross-section of HP1 sample after failure near the stress concentration

to distinguish the location of the change in resistances measured with position on the sample, the DP samples consistently showed accumulation of mechanical damage beyond strains of piezoresistivity for CNTs. A disadvantage of this method is, comparing the stress curves of the control and CNT patch DragonPlate samples, the CNT patch appears to influence the mechanical behavior of the sample, and so may not be a pure reflection of the mechanical health of the sample itself. Nvertheless, of particular note is the capabilty of such CNT patches as effective strain gauges to detect accumulation of damage over the tested lifetime of the sample. Because these CNT patches are only adhered to the surface of the sample, they can be easily integrated into existing materials and accelerate the process of structural health monitoring.

3.2 Damage Sensing in Hexcel samples

The Hexcel structures (HP and HC) tested consisted of Hexcel prepreg laminated into 16 layers with unidirectional aligned CNTs knocked-down and adhered to the outer surfaces. The motivation for testing such a structure is eventual evaluation of damage sensing in nanostitch samples due to its improved interlaminar reinforcement of composites. The Hexcel structures would represent the first structure in this investigation with anistropies due to the repeating orientation of the unidirectional layers, and in future work with nanostitching, a structure with integrated CNTs. Additionally, due to the simple geometry at which the knocked-down surface CNTs are added, the manufacturing of such nanostitch composites adds only a few steps to existing practices in inudstry. Because the HP and HC samples have CNTs integrated within the structure, all samples apart from two control samples are grid (G) configuration. A total of 9 samples were tested; five with knocked down aligned CNT patches adhered to the surface and five without. Of the five without, two were in G configuration, one in H configuration, and one in V configuration.

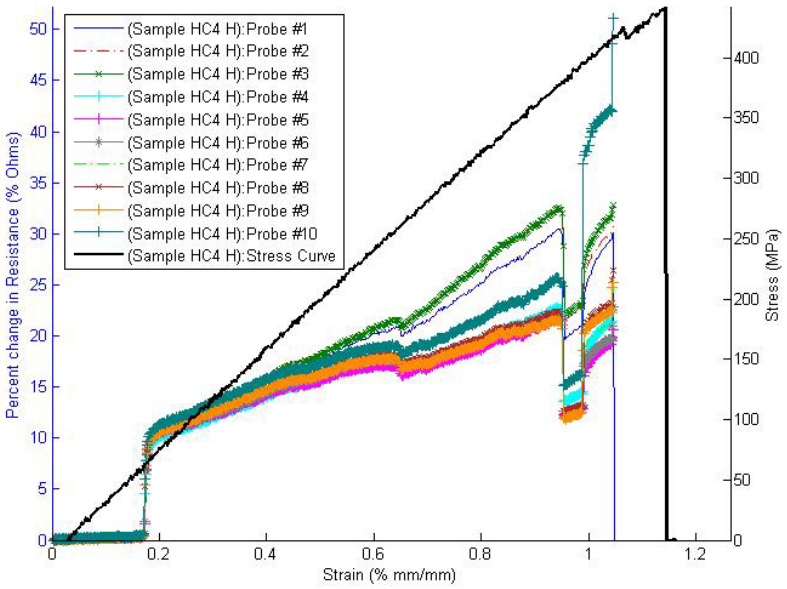

Figure 23: Example of overlayed stress curve with measured changes of resistance for HC4 control sample without CNT patches

Of the control samples, HC1 and HC2 were in G configuration. Due to slipping problems, the data for sample HC1 revealed very little about the sample and so was disregarded. Sample HC2 had similar mechanical behavior to all other Hexcel samples, but the recorded resistance data illustrated very little and may be found in Appendix C with the plots of the remaining HC samples. The remaining HC samples, HC3 and HC4 in V and H configuration respectively showed some promise in damage sensing, in that the resistances measured did monotonically but not consistently increase as with the DragonPlate samples, as illustrated in Fig. 23. The contrast between the HC samples in H,V and G configurations suggests that the H and V configuration is more appropriate with usage of the CNT patch, instead of the G configuration. This may be due to the fact that carbon fiber through the thickness of the sample provides unintended alternate conductive paths for the current to flow through, apart from the CNT patch, and introduces noise in the measured resistance. However, since the mechanical behavior and measured electrical resistances were significantly different from the remaining Hexcel samples, such conclusions are tenuous and would require further investigation with computational methods that are able to detangle local strain damage to changes in the conductive network. The control nevertheless illustrates that the CNT patch as a strain gauge applies to a variety of composite structures. All plots are overlay of strain (% mm/mm) with percent change in resistance (% Ohms) and stress (MPa).

Apart from the control samples, the mechanical behavior of the Hexcel samples with CNT patches was consistent across samples, which ranged between 1.0-1.5% elongation strain. Most samples tested failed at around 450 GPa. The only sample that exhibited the onset of increasing compliance was HC1, as it was the only sample to reach a strain beyond 1.5% elongation, which is approximately where most DragonPlate samples began to inelastically deform. For the majority of the sample test, the HP samples appear to remain mostly linear before failure; extrapolating other mechanical behaviors in the HP samples would be ambiguous.

Fig. 24 presents the change in electrical resistance measurements for several of the HP samples tested in the far field area of the probes indicated. Sample HP5 is not shown due to the fact that the resistances measured show no correlation with the mechanical data, but is included in Appendix C. Unlike the DragonPlate samples, there are few characteristics similar across all samples and there are few changes in the stress curves to lend any correlation with what happening mechanically. However, several key aspects can be discerned.

As Fig. 24 illustrates, although little can be discerned based of the load curve, several key features of the Hexcel samples are revealed. This is most evident with Sample HP2. There are two regions in Figs. 24b and 24c that border along around 0.6% strain and 0.8% strain respectively, which suggests possible mechanical damage accumulation similar to that of the DragonPlate samples. Given that there is little to correlate between the stress curve and measured resistance, it is not possible to establish with certainty whether this is the case. Most of the samples failed when the change in resistance reached between 1.5-4.0% change in Ohms. Given that this is close to the change in resistance from the inherent piezoresistivity of CNTs, the ability to discern the structural health of a Hexcel sample with a CNT patch on the surface is less defined. The HC control samples illustrated that a knocked-down surface CNT patch preserves similar electrical resistance measurements to the DragonPlate samples, in that the changes in resistance monotonically increase and increase in distinct jumps, but this was immediately lost when additionally introducing CNTs through the thickess of the sample, when measurements were done through the thickness of the sample. This would suggest that then the measurements would be dependent on the local topography of the CNT or CF network and the quality of alignment at which CNT is stitched into the structure or the integrity of the unidirectional CF layer. Thus, the variability of manufacturing each sample with CNTs manifested in the wide variety of change in resistance curves and the large ranges of changes in resistanes at failure seen in the samples. These suggest that combining CNTs as both a surface strain gauge and as an internal sensor interfere with each other and result in variance. In order to fully evaluate the merits of

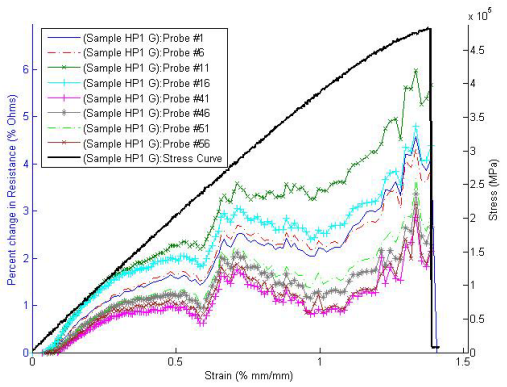

(a) Correlation of stress and total measured changes in electrical resistance for sample HP1

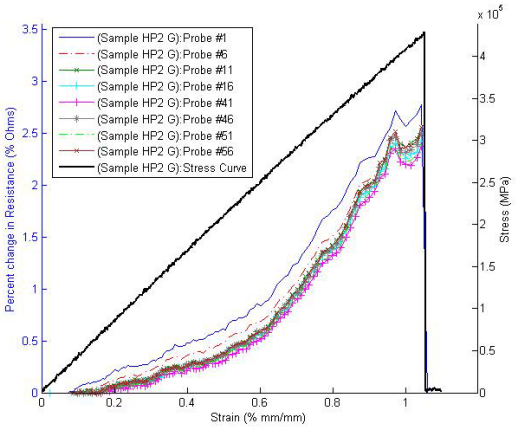

(b) Correlation of stress and total measured changes in electrical resistance for sample HP2

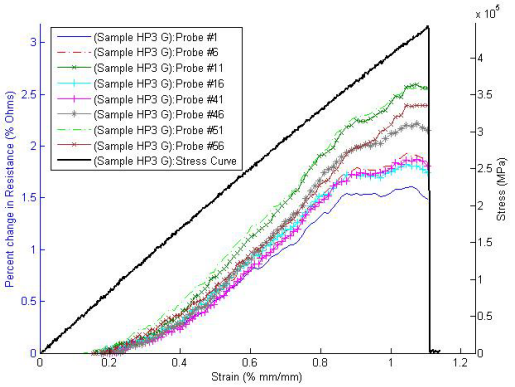

(c) Correlation of stress and total measured changes in electrical resistance for sample HP3

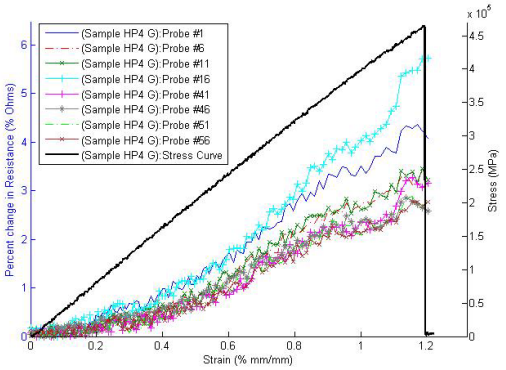

(d) Correlation of stress and total measured changes in electrical resistance for sample HP4

Figure 24: Overlayed stress curve with total measured resistance changes for HP samples in G configuration; all graphs are from the same locations on the sample, correlating with far field resistance measurements

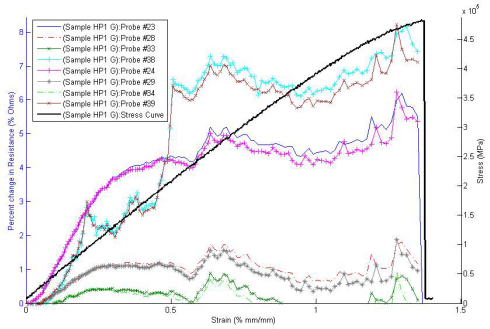

(a) Correlation of stress and measured changes in electrical resistance for sample HP1

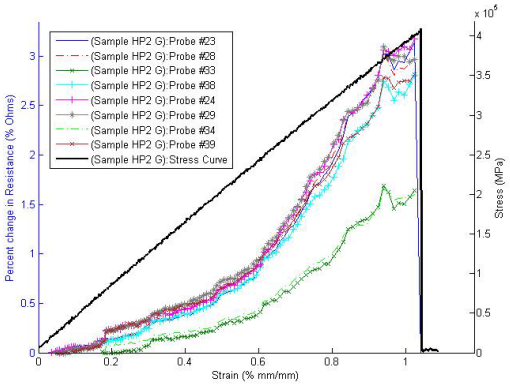

(b) Correlation of stress and measured changes in electrical resistance for sample HP2

Figure 25: Correlation of stress and total measured changes in electrical resistance for samples HP1 and HP2, reinforcing the lack of measured consistency across resistance measurements with mechanical damage accumulation near the stress concentration

combining multiple CNT network topographies, the HP samples would need to undergo loading in which plastic deformation occurs in order to determine if the CNT network also acculumates damage with the sample, and a greater number of control samples need to be tested in order to establish consistency between measurements and elucidate the influence of the surface CNT patch on the measured electrical resistance.

In terms of consistency around specific areas with respect to the stress concentration, Fig. 24 also suggests a lack of similarity of the change in electrical resistance measured across samples. Although sample HP2 demonstrates considerable consistency of changes in electrical resistance for even measurements in different areas across sample, sample HP1 does not maintain any consistency, even within the same proximity to the stress concentration, and this is lost completely when approaching the stress concentration where the larger stresses accentuate the local deformation of the material and thus local readings of the electrical resistance, as shown in Fig. 25

Further investigation is needed to fully evaluate the capabilities of the nanostitching CNTs as damage and damage accumulation sensors in conjunction with the surface CNT patch. Future work would consider nanostitching between each interface and evaluating the ability of this particular CNT network to detect damage. The current data presents inconclusive evidence and suggests opposite interpretations of the the Hexcel structures to also be able to be used as also a method of self-diagnosis. In order to better evaluate the non-destructive evaluation and damage sensing abilities of the nanostitch CNTs, the possible conductive pathways between the CNT patches and CFs must be considered in future work. The stability of the data suggest that using a surface CNT patch as with the DragonPlate samples are equally as effective.

3.3 Damage Sensing in FFRP samples

The fuzzy fiber reinforced plastic (FFRP) composite samples consist of fully integrated aligned CNTs in the structure, as mechanism for both interlaminar and intralaminar reinforced against crack propagation. CNTs are grown radially around the fibers of a woven cloth substrate. For sufficiently long CNTs above the percolations threshhold (greater than 10 microns), the CNTs are able to effectively percolate and bridge across fibers both within and between layers. FFRP samples represent further integration of CNTs in composite structures. The motivation for investigating these samples is to evaluate whether CNTs are able to function both as mechanical reinforcement and as strain or damage sensors.

As all samples had CNTs integrated throughout the sample, FFRP samples were grid configured. No FFRP samples had CNT patches adhered to the surface. Five samples in total were made. Each sample had a different weight percent gain of CNTs, defined as the quotient of the gain in weight from CNT growth and the original weight of the substrate cloth with catalyst. The corresponding weight gains and the actual weight gains of each ply may be found in Appendix A, and are correlated with average CNT length.

The mechanical behavior of the FFRP samples looked similar. All samples manufactured failed at around 0.7-0.9% elongation strain and 110-150 MPa stress. Unlike the DragonPlate samples, the FFRP samples did not exhibit significant change in compliance throughout the duration of the tensile tests. The mechanical behavior of FFRP samples was therefore more repeatable in comparison to the other sample types tested. Of additional note is that the open-hole tensile mechanical properties are not significantly altered by the weight gain of the sample. The hypothesis is that longer CNTs correlate with larger weight gains, and longer CNTs are able to better percolate and bridge across fibers. Additionally, as know through the shear-lag model, the CNTs must be above a critical length in order to percolate through the matrix and to avoid CNT pullout as a failure mechanism. However, these greatly depend on the growth conditions present during the growth of CNTs on the plies used in the FFRP laminate structure. In order to determine whether the aforementioned hypothesis is valid, characterization of the plies grown were characterized by length using an SEM. Due to varied growth conditions, different growth lengths and morphologies resulted. Characterization of these morphologies and lengths may be found in Appendix B. In order to achieve the desired weight gain of CNTs, the growth time in which ethylene and hydrogen are flowed is adjusted. In general, the correlation between CNT length and weight percent gain did not significantly affect the damage sensing capabilities across the FFRP samples. The data Appendix B covers the span of weight gains used in this study.

Because the FFRP samples were not as significantly strained beyond typical values for deformation beyond typical piezoresistivity measurements, which are on the order of 0.5% strain for other systems with

CNTs as sensors in various composite structures, determining whether the FFRP CNT network reflects the accumulation of damage of the sample is less definitive. Thus, numerical fitting methods are employed in order to quantitatively determine if the CNT network in the FFRP samples accumulate damage with the mechanical deformation of the sample. Depending on the arrangement and loading of CNTs in the sample, the upper limit of strain of the CNT inherent piezoresistivity varies substantially. To determine the approximate strain at which the change of measured electrical resistnace is meaninfully correlated to damage or damage acculumation, it is demonstrated that the FFRP samples measured consistent electrical resistance changes for similar locations on the sample and that beyond a certain strain, these diverge, indicating the concentration of the accumulation of mechanical damage that is not predicted with piezoresistivity alone. Fig. 26 demonstrates this with selected FFRP samples. A full list of FFRP sample plots may be found in Appendix C. All plots are overlay of strain (% mm/mm) with percent change in resistance (% Ohms) and stress (MPa).

As seen in Fig. 26, there is a sustained consistency of electrical resistance change far from the stress concentrator when comparing the probes for far and near the stress concentration. Particularly noteworthy is the divergence that occurs in the near field measurements. As the FFRP samples consist of radially grown CNTs on woven cloth, the laminate may be abstracted as quasi-isotropic. That is, it is hypothesized that due to the radially dispersion of CNTs in the composite, the meausured piezoresivitivity of the CNTs themselves would be consistent regardless of the direction of applied stress. Thus, the divergence indicates a different mechanism of mechanical damage. Indeed, during tensile testing, before the FFRP samples failed, in the latter half of the test, crackling sounds could be heard from the samples, indicative of fiber and matrix damage accumulation prior to ultimate failure. Fig. 27 shows several failure mechanisms in the cross section of the area of failure near the hole.

Combining these observations, it is taken by convention for the FFRP samples that the onset of mechanical deformation beyond the inherent piezoresitivity of the CNTs in the FFRP samples occurs approximately midway in the sample test at approximately 0.25% strain. This convention is taken, as it is the point before electrical measurements in the probes begin to consistenly diverge among the samples, which may be indicative of local damage. Although the images of sample failure and general test observations indicate mechanical damage beyond elasticity that the probes may reflect, this is further suggested using statistical fitting methods for the various measurements conducted across each FFRP sample. A curve is first fitted to a selected probe and compared to other neighboring probes measuring the resistance in the same relative proximity to the stress concentration for the first 0.25% strain the sample experiences, denoted as the trun-

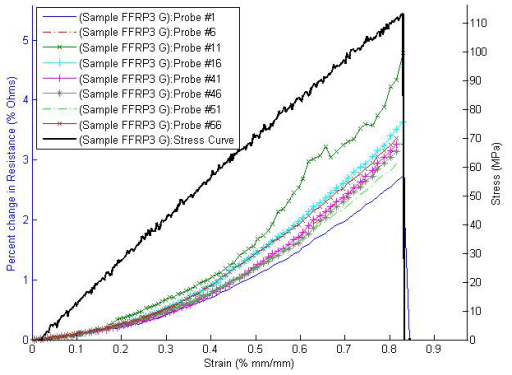

(a) Correlation of stress and changes in electrical resistance for sample FFRP3, 3wt%, far field measurements

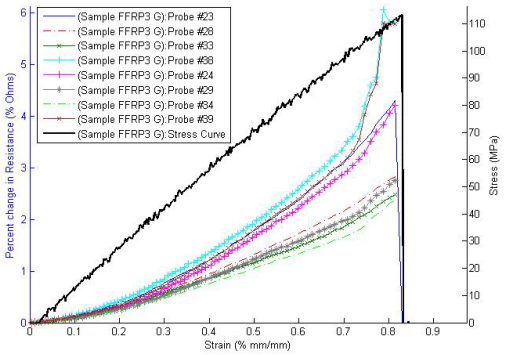

(b) Correlation of stress and changes in electrical resistance for sample FFRP3, 3wt%, near field measurements

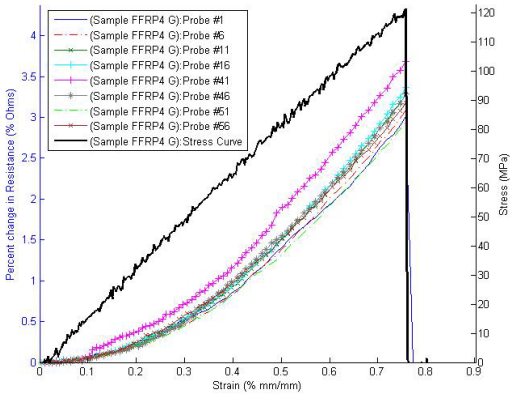

(c) Correlation of stress and changes in electrical resistance for sample FFRP4, 4wt%, far field measurements

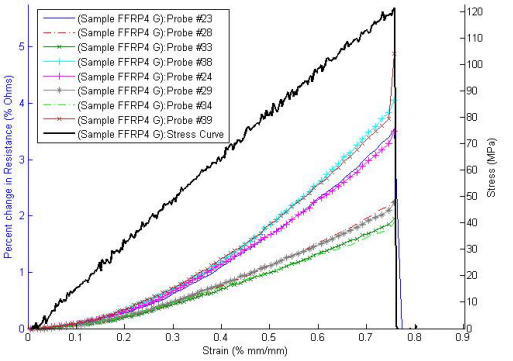

(d) Correlation of stress and changes in electrical resistance for sample FFRP4, 4wt%, near field measurements

Figure 26: Correlation of stress and total measured changes in electrical resistance for selected FFRP samples demonstrating consistency of electrical resistance changes far from the hole and divergence near the stress concentration

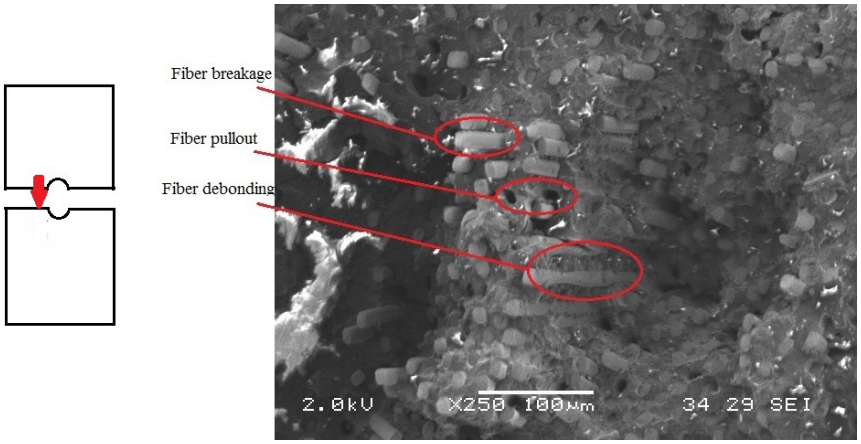

Figure 27: SEM image of the cross section of the location of failure for FFRP4 demonstrating several modes of laminate failure

cated strain curve. This same curve is then compared to a raw data of the same probe for the sample for strain until failure, denoted as the raw curve. Fig. 28 demonstrates an example of this method. The probe that is selected is chosen by convention to be Probe 23 near the stress concentration; probes further away from the stress concentration show no divergence of electrical resistance measurements to the extent that probes near the stress concentration do.

The goodness of the fits used are determined using the R-square and RMSE (root mean square error) statistical metrics. R-square, better known as the coefficient of determination, is a measure of how well the modeled curve aligns with the data given. The RMSE is the mean square error, and is a measure of the total deviation of the model with the inputted data. The lowest R-square value for the model fits was 0.98; most R-square models used were approxiately 0.99. Given that measurements far from the hole are more consistent than near the hole, the aforementioned fitting method does not indicate the accumulation of damage. For the near hole measurements, the divergence emerges due to the relative proximity to the stress concentration. It has been analytically shown in elastic theory that circular holes result in a stress concentration factor of three in isotropic materials. That is the applied stress is amplied by a factor of three in the area immediately near the hole and falls off exponentially. A similar effect would be expected in anisotropic materials such as the composites tested. The divergence occurs between the selected probes near the hole. The probes selected for the shown near hole measurements comprise of measurements closest to the hole and the measurements of probes adjacently located. The divergence between measurements occurs near the hole in the probes second closest to the hole, indicating accumulation of damage due to proximity to the stress concentration. Particularly interesting is that these are not the measurements closest to the

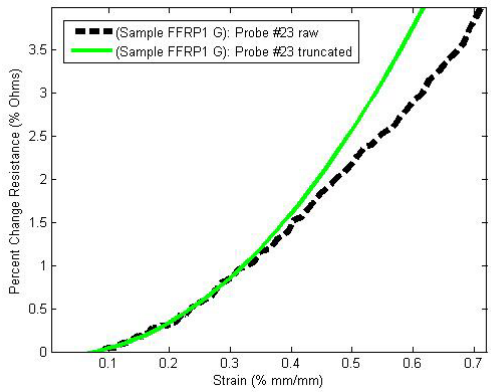

(a) Comparison for FFRP1 of the truncated strain and raw strain curves, in near field probe 23

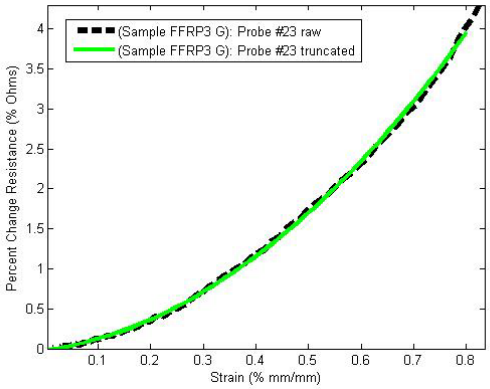

(b) Comparison for FFRP3 of the truncated strain and raw strain curves, in near field probe 23

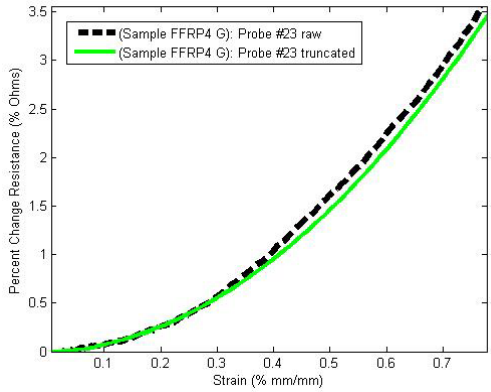

(c) Comparison for FFRP4 of the truncated strain and raw strain curves, in near field probe 23

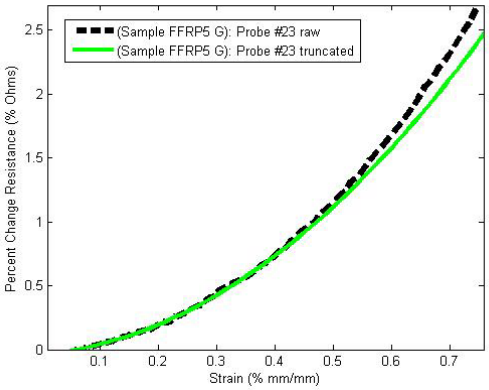

(d) Comparison for FFRP5 of the truncated strain and raw strain curves, in near field probe 23

Figure 28: Comparing the truncated strain curve and raw strain curve in FFRP samples for determining if mechanical damage accumulation is reflected in the probes; some samples that do no show zero resistance at 0% strain are due to faulty probes that measured initially slighltly negative resistances

stress concentration. A possible explanation is that these measurements were too close to the hole where it was cut and reamed smooth, thus altering the local material properties. Nevertheless, it is hypothesized that the point of divergence between probes indicates accumulation of mechanical damage and correlates with acoustic events that occurred during testing.

Modeling the probe with the largest change in resistance in the FFRP samples most easily captures the potential of the mechanical damage accumulation for high stresses beyond the failure stress of the sample overall. Fig. 28 captures example probes of the samples that exhibited the most consistent change in resistance for a particular location relative to the location of the stress concentration. As seen in this figure, there is a small indication that damage accumulation occurs at the point of divergence for a particular probe as suggested earlier in the range of strains tested. A possible explanation may be that although the individual fibers failed, the radial interpenetration of CNTs throughout the resin network provides a multitude of alternative conductive pathways for current to pass, to the effective resistance measured does not percievably change significantly. Additionally, the divergence occurs in both directions. That is, the measured electrical resistance grows faster than predicted in the aforementioned determined range for piezoresistivity for some samples but not consistently among all samples. This suggests that the probes are measuring some kind of damage or damage accumultion but that it is dependent on locality. A possible microstructure argument is that the CNTs may pull apart or relax upon pull out or breakage respectively, depending on the mode of failure. Other methods of mechanical loading, such as purely tensile testing, may be necessary to definitively evaluate the self-diagnosing capabilities of the CNTs in FFRP samples. These data suggest that through-thickness measurements of resistance for non-destructive evaluation of a structure is dependent on if the probe is near the stress concentration and may not as appropriate for damage detection for this particular CNT network architecture as other previously demonstrated methods as [57].

3.4 Evaluation of Damage Sensing Capabilities of CNTs

A major component of damage sensing to understand is that many of the conclusions drawn from samples are like those in fractography, the study of failure in mechanically loaded structures; they are inferrences from the data. The range of samples tested showed promise of CNTs as damage and damage accumulation sensors. However, as seen through the Hexcel and FFRP samples, the arrangement and topography of the CNT network plays a significant role in the efficacy of the CNTs as a mechanical damage sensor. The samples tested emphasize the need to optimize the topography of the CNT network, such that there are limited number of conductive pathways for current to flow through while simulataneously being able to

transmit mechanical damage accumulation to areas far from the stress concentration or potential point of failure.

The DragonPlate and Hexcel samples demonstrated that CNT patches as material strain surface gauges worked effectively as a self-diagnosis tool, when computing the change in electrical resistance of the patch. It has been shown through several samples, that critical points in the mechanical stress curve correlate with particular characteristics of the change in the electrical resistance. Several things are noteworthy. Both the DrgaonPlate and Hexcel samples with CNT patches that measured resistance changes across the surface of the CNTs themselves showed consistency and correlation between the mechanical load and electrical resistance curves. The Hexcel samples with resistances measured through the thickness of the sample in grid configuration suggested that even with the insulating adhesive layer, having the CNT patch in G configuration resulted in too inconsistent readings that were potentially dependent on the local arrangement of the CF or CNT network. This was reflected in the control Hexcel samples measured with G configuration in comparison to the H and V configured HC samples, shown in Appendix C. Thus, the DragonPlate and Hexcel samples suggest that unidirectional knocked down CNTs as a material strain gauge is effective as a damage sensor, and potentially a structural health monitoring tool. Overall, the DragonPlate and Hexcel samples emphasize the importance of the CNTs creating a continuous conductive network with the appropriate topography to be utilized as a sturctural health monitoring tool.

The FFRP samples demonstrated that although radially dispersed CNTs are useful for localizing where damage occurs, it does not disperse the effects of mechanical damage accumulation to other areas. Moreover, the samples tested did not seem to accumulate damage as definitively as the previous samples, and so were inconclusive. Nevertheless, the FFRP samples demonstrated that consistency between samples is achievable using integrated CNTs in the composite structure.

3.5 Further Investigation

There are several aspects in this project for improvement and further investigation. As many of the silver paint probes often failed before the sample, choosing a more consistent material and process for the probes that simulataneously interferes little with the mechanical tests, such as copper mesh, would be needed. This would additionally minimize the amount of electrical noise that appeared in the data. Manufacturing more control samples would also provide more data and understanding of the inherent failure resistance changes in the silver paint alone, and help decouple the changes in resistance from the sample, from the CNTs included in the system, and from the silver paint probes themselves. Given that little additional

information was gathered from collecting data at such close intervals, measuring resistances across select areas of interest would be more efficient and provide further evidence to the utility of aligned CNTs as damage or damage acculumation sensors. Additionally, conducting the full implementation of the Hexcel samples with nanostitching would provide insight to how the CNT network architecture as layers of aligned CNTs affects the measured resistance.

Furthermore, the strains at which Hexcel and FFRP samples failed and corresponding data suggested that little mechanical damage accumulation occurred in the sample before failure, indicating that the size or presence of the hole prematurely caused the samples to fail before further insightful data could be collected. Thus, a future modification could be various other mechanical tests, such as simple tensile or 3- and 4-point bending tests, or modifying the size of the hole to scale with the failure strength of each sample. Additionally, the choice of open-hole tensile testing is not accurately reflective of the typical mechanical lifetime of a structural part in industry. In order to better simulate what a composite structure experiences over its lifetime and the corresponding monitoring over time, cyclic loading and fatigue tests could be conducted. Additionally, conducting environmental tests where the samples are subjected to humidity, atmospheric, and temperature conditions to that of an aerospace structure as done in [62] would also provide a more accurate picture to the damage sensing capabilities of CNTs in the proposed architectures. This would require using probes that are more environmentally resistant, as noted in [62], and presents an additional aspect of investigation for future studies. Further possibilities are using a multiscale approach to decouple different mechanisms for mechanical damage acculumation in the CNT networks. Additional studies would be to use AC, rather than DC to measure the impedance response of the samples using impedance spectroscopy to better understand the electrical response of the CNT network.

Additonal areas of investigation would be to construct particular architectures of the CNTs. The architectures tested represent a small fraction of the possible architectures. For example, using randomly aligned CNT patches instead of unidirectionally knocked down ones would help decouple the effect of network topography from the inherent structural health monitoring capabilities of CNTs. Furthermore, it provide a bridge between much of the analysis hypothesized in this study between samples of different CNT architectures.

In terms of areas of further investigation, more computational methods need to be developed. In general, the field of fractography and study of failure is still in its initial developmental stages. Because structures on the laminate scale are capable of failing from a myriad of mechanisms, ranging from delamination to fiber breakage that can occur over a length of time, the predicative power of analytical models for laboratory or industrially made samples is extremely limited. However, using numerical methods that would be able

to characterize these modes of failure and provide probabilistic metrics for failure would provide a more microstructure method of understanding failure and provide a more systematic means of manipulating the CNT such that its full material advantages are highlighted.

4 Conclusions

Three types of samples were tested in order to evaluate the damage and damage accumulation sensing capabilities of aligned carbon nanotubes (CNTs). The first type was the industrially purchased quasi-isotropic graphite DragonPlate that was tested with a unidirectional knocked-down CNT patch adhered to the surface as a strain gauge. The second type was of laminate composite architecture with unidirectional plies in various orientations, in which CNTs are integrated onto the surface of the composite. The third sample was fuzzy fiber reinforced plastic (FFRP) laminated composites, which have fully integrated CNTs radially grown on fibers in a woven substrate. Each sample type represented a varying degree to which CNTs were integrated into the structure. These samples were then tested in open-hole tension while simultaneously measuring the electrical resistance. The following were concluded from the data collected, as sorted by sample type.

- The industrially purchased DragonPlate samples with unidirectional knocked down CNT patches adhered to the surface demonstrated the clearest distinction between CNT network piezoresitivity in which the CNT network deforms reversibly and mechanical damage accumulation. However, the change in resistance between even probes within each others vicinity on the sample was not consitent and ranged between 20-120% resistance change in Ohms, indicating variability in the manufacturing of the probes. These samples indicates that the CNT patches provide clear but not quantitatively consistent electrical resistance readings. This suggests that the CNT patches are useful for quick diagnosis of a structural part that requires knowledge of its previous mechanical history, but that there is little correlation between a particular change in resistance and strain. However, these samples provide a useful basis for evaluating CNT patches as a bridge between current damage sensing techniques to structural health monitoring with CNTs.

- The Hexcel prepreg carbon fiber demonstrated less consistency between samples but much greater consistency within each sample in comparison to the DragonPlate samples in terms of the overall shape of the change in resistance curve and magnitude. Additionally the total change in resistance was less dramatic and constrained to at most 8% change in Ohms. Samples without the CNT patch demonstrated probe behavior similar to those of the DragonPlate samples when H or V configuration, but were not as meaningful in G configuration. The smaller percent change in resistance may be due to the sample prematurely failing from the stress concentration, and would require additional testing.

- The FFRP laminate composites consisted of radially grown CNTs on a woven ceramic fabric and

manufactured as layered plies. Like the Hexcel samples, the FFRP samples reached a low strain, consistently below 1.0% strain, also possibly due to premature failure. The FFRP samples showed the greatest amount of consistency within and between samples of the sample types tested, which may be attributed to the more isotropic distribution of CNTs in the structure. Typical change in resistance values were around 5.0% change in Ohms. However, as determined using statistical fits, it is suggested that for the tests conducted in this investigation, a majority of the CNT network deformation was network piezoresistivity, as there is little divergence between the initial part of the data and remaining data. The divergence indicates a weak ability of the FFRP construction of CNTs to reflect mechanical damage accumulation in the sample, particularly far from regions of local damage. However, given that FFRP samples demonstrated the greatest consistency, further testing and investigation is warranted for this particular CNT network architecture.

Overall, it was found that CNTs in unidirectional knocked down patches as material strain gauges were effective at reflecting mechanical damage accumulation across several samples and sample types, but was not consistent in measurement. That is, probes often failed prematurely or measured radically different changes in electrical resistance, such that it is not possible to correlate a change in resistance with an inelastic strain. Furthermore, the consistency of the electrical resistance measurements from the probes varied between samples and among sample types, particularly among the DragonPlate samples. Using fully integrated CNTs in the conformation in the FFRP samples showed limited promise to show accumulation of damage far from stress concentrations but was more promising in terms of reflecting mechanical damage locally, as seen with thermographic and tomographic methods.

The choice of these samples highlight the importance of the architecture of the CNT network. This investigation suggests that having a CNT network selectively percolating through the network in a less stochastic way is important in order to get meaningful structural health monitoring diagnoses far away from local damage. The results of this investigation indicate that aligned CNTs as damage or damage acculumation sensors show protential for non-destructive evaluation and promise for structural health monitoring. Thus, in order to take advantage of CNTs superior mechanical and electrical properties for both mechanical reinforcement and structural health monitoring, the architecture of the CNT network must be engineering such that both are optimized.

5 Acknowledgements

Thank you to those at Metis Design, Corp. and Dr. Samuel Buschhorn for helping to make samples and helping to test the samples. Additionally, thank you to Sunny Wicks for helping to teach how to make FFRP samples and being a terrific UROP mentor, and Professor Brian Wardle and Professor Jeffrey Grossman for providing advice and guidance throughout the project.

This work made use of the MRSEC Shared Experimental Facilities at MIT, supported by the National Science Foundation under award number DMR-08-19762.

References

[1] G. Nessim, "Properties, synthesis, and growth mechanisms of carbon nanotubes with special focus on thermal chemical vapor deposition," *Nanoscale*, vol. 2, pp. 1306–1323, 2010.

[2] L. de Technologie des Composites et Polymères. (May 2012) Research. http://ltc.epfl.ch/page-59327-fr.html. É cole Polytechnique Féderale de Lausanne.

[3] B. Verijenko and V. Verijenko, "A new structural health monitoring system for composite laminates," *Composite Structures*, vol. 71, pp. 315–319, 2011.

[4] R. Silva-Muñoz and R. Lopz-Anido, "Structural health monitoring of marine composite structural joints using embedded fiber bragg grating strain sensors," *Composite Structures*, vol. 89, pp. 224–234, 2009.

[5] H. Li, I. Herszberg, C. Davis, A. Mouritz, and S. Galea, "Health monitoring of marine composite structural joints using fibre optic sensors," *Composite Structures*, vol. 75, pp. 321–327, 2006.

[6] X. Zhao, R. Royer, S. Owens, and J. Rose, "Ultrasonic lamb wave tomography in structural health monitoring," *Smart Materials and Structures*, vol. 20, 2011.

[7] R. Belchamber, D. Betteridge, Y. Chow, T. Lilley, M. Cudby, and D. Wood, "Evaluation of pattern recognition analysis of acoustic emission from stressed polymer and composites," *Journal of Acoustic Emissions*, vol. 4, pp. 71–83, 1985.

[8] J. Coleman, U. Khan, W. Blau, and Y. Gun'ko, "Small but strong: A review of the mechanical of carbon nanotube-polymer composites," *Composites Science and Technology*, vol. 70, pp. 1–19, 2010.

[9] S. Iijima, "Helical microtubules of graphitic carbon," *Nature*, vol. 354, pp. 56–58, 1991.

[10] R. Brukh and S. Mitra, "Mechanism of carbon nanotube growth by cvd," *Chemical Physics Letters*, vol. 424, pp. 126–132, 2006.

[11] G. Che, B. Lakshmi, C. Martin, and E. Fisher, "Chemical vapor deposition based synthesis of carbon nanotubes and nanofibers using a template method," *Chem. Mater.*, vol. 10, pp. 260–267, 1998.

[12] A. Gohier, C. Ewels, T. Minea, and M. Djouadi, "Carbon nanotube growth mechanism switches from tip- to base-growth with decreasing catalyst particle size," *Carbon*, vol. 46, pp. 1331–1338, Aug 2008.

[13] M. Kumar, "Carbon nanotube synthesis and growth mechanism," in *Nanotechnology and Nanomaterials*, S. Yellampalli, Ed. InTech, July 2011, ch. 8.

[14] K. Raji, S. Thomas, and C. Sobhan, "A chemical kinetic model of chemical vapor deposition of carbon nanotubes," *Applied Surface Science*, vol. 257, pp. 10 562–10 570, 2011.

[15] E. Minot, "Tuning the band structure of carbon nanotubes," Ph.D. dissertation, Cornell University, August 2004.

[16] P. Bandaru, "Electrical properties and applications of carbon nanotube structures," *Journal of Nanoscience and Technology*, vol. 7, pp. 1–29, 2007.

[17] H. Dodziuk and G. Dolgonos, "Molecular modeling study of hydrogen storage in carbon nanotubes," *Chemical Physics Letters*, vol. 356, pp. 79–83, April 2002.

[18] H. Peng, D. Chen, J. Huang, S. Chikkannanavar, J. Haenisch, M. Jain, D. Peterson, S. Doorn, Y. Lu, Y. Zhu, and Q. Jia, "Strong and ductile colossal carbon tubes with walls of rectangular macropores," *Physical Review Letters*, vol. 101, p. 145501, 2008.

[19] B. Dumé. (Aug 2008) Carbon nanotubes, but without the 'nano'. http://physicsworld.com/cws/article/news/2008/aug/08/carbon-nanotubes-but-without-the-nano. Institute of Physics.

[20] T. Chou, L. Gao, E. Thostenson, Z. Zhang, and J. Byun, "An assessment of the science and technology of carbon nanotube-based fibers and composites," *Composites Science and Technology*, vol. 70, pp. 1–19, 2010.

[21] D. Chung, "Carbon materials for structural self-sensing, electromagnetic shielding and thermal interfacing," *Carbon*, vol. 50, pp. 3342–3353, 2012.

[22] E. Thostenson and T. Chou, "Carbon nanotube-based health monitoring of mechanically fastened composite joints," *Composites Science and Technology*, vol. 68, pp. 2557–2561, 2008.

[23] K. Kim, W. Yu, J. L. nad L Gao, E. Thostenson, T. Chou, and J. Byun, "Damage characterization of 3d braided composites using carbon nanotube-based *in situ* sensing," *Composites Part A: Applied Science and Manufacturing*, vol. 41, pp. 1531–1537, Oct 2010.

[24] M. Nofar, S. Hoa, and M. Pugh, "Failure detection and monitoring in polymer matrix compoistes subjected to static and dynamic loads using carbon nanotube networks," *Composites Science and Technology*, vol. 69, pp. 1599–1606, Aug 2009.

[25] L. Gao, T. Chou, E. Thostenson, Z. Zhang, and M. Coulaud, "*In situ* sensing of impact damage in epoxy/glass fiber composites using percolating carbon nanotube networks," *Carbon*, vol. 49, pp. 3382–3385, Aug 2011.

[26] J. Abot, Y. Song, M. Vatsavaya, S. Medikonda, Z. Kier, C. Jayasinghe, N. Rooy, V. Shanov, and M. Schultz, "Delamination detection with carbon nanotube thread in self-sensing composite materials," *Composites Science and Technology*, vol. 70, pp. 1113–1119, 2010.

[27] C. Li and T. Chou, "Modeling of damage sensing in fiber composites using carbon nanotube networks," *Composites Science and Technology*, vol. 68, pp. 3373–3379, 2008.

[28] D. Wang and D. Chung, "Through-thickness stress sensing of a carbon fiber polymer-matrix composite by electrical resistance measurement," *Smart Materials and Structures*, vol. 16, pp. 1320–1330, 2007.

[29] Z. Xia and W. Curtin, "Modeling of mechanical damage detection in cfrps via electrical resistance," *Composites Science and Technology*, vol. 67, pp. 1518–1529, 2007.

[30] Y. Kuronuma, T. Takeda, Y. Shindo, F. Narita, and Z. Wei, "Electrical resistance-based strain sensing in carbon nanotube/polymer composites under tension: Analysitcal modeling and experiments," *Composites Science and Technology*, vol. 72, no. 14, pp. 1678–1682, Sept 2012.

[31] X. Fu, W. Lu, and D. Chung, "Ozone treatment of carbon fiber for reinforcing cement," *Carbon*, vol. 36, no. 9, pp. 1337–1345, 1998.

[32] Y. Xu and D. Chung, "Cement-based materials improved by surface treated admixtures," *ACI Mater J*, vol. 97, no. 3, pp. 333–342, 2000.

[33] D. Chung, "Dispersion of short fibers in cement," *J Mater Civil Eng*, vol. 17, no. 4, pp. 379–383, 2005.

[34] S. Wen and D. Chung, "Strain sensing characteristics of carbon fiber reinforced cement," *ACI Mater J*, vol. 102, no. 4, pp. 244–248, 2005.

[35] N. Alexopoulos, C. Barholome, P. Poulin, and Z. Marioli-Riga, "Structural health monitoring of glass fiber reinforced composites using embedded carbon nanotube (cnt) fibers," *Composites Science and Technology*, vol. 70, pp. 260–271, 2010.

[36] J. Rausch and E. Maeder, "Health monitoring in continuous glass fibre reinforced thermoplastics: Manufacturing and application of interphase sensors based on carbon nanotubes," *Composites Science and Technology*, vol. 70, pp. 1589–1596, 2010.

[37] B. Fankhaenel, E. Mueller, U. Mosler, and W. Siegel, "Sic-fibre reinforced glasses - electrical properties and their application," *Journal of the European Ceramic Society*, vol. 21, no. 5, pp. 649–657, May 2001.

[38] L. Boeger, M. Wichmann, L. Meyer, and K. Schulte, "Load and health monitoring in glass fibre reinforced composites with an electrically conductive nanocomposite epoxy matrix," *Composites Science and Technology*, vol. 68, no. 7-8, pp. 1886–1894, 2008.

[39] W. Luheng, D. Tianhuai, and W. Peng, "Influence of carbon black concentration on piezoresistivity for carbon-black filled silicone rubber composite," *Carbon*, vol. 47, pp. 3151–3157, 2009.

[40] C. Li, E. Thostenson, and T. Chou, "Sensors and actuators based on carbon nanotubes and their composites: A review," *Composites Science and Technology*, vol. 68, pp. 1227–1249, 2008.

[41] J. Ku-Herrera and F. Aviles, "Cyclic tension and compression piezoresistivity of carbon nanotube/vinyl ester composites in elastic and plastic regimes," *Carbon*, vol. 50, pp. 2592–2598, 2012.

[42] S. Wen and D. Chung, "Model of piezoresistivity in carbon fiber cement," *Cement and Concrete Research*, vol. 36, pp. 1879–1885, 2006.

[43] N. Hu, Y. Karube, C. Yan, Z. Masuda, and H. Fukunaga, "Tunneling effect in a polymer/carbon nanotube nanocomposite strain sensor," *Acta Materialia*, vol. 56, pp. 2929–2936, 2008.

[44] T. Theodosiou and D. Saravanos, "Numerical investigation of mechanisms affecting the piezoresistive properties of cnt-doped polymer using multi-scale models," *Composites Science and Technology*, vol. 70, pp. 1312–1320, 2010.

[45] S. Zhu and D. Chung, "Analytical model of piezoresistivity for strain sensing in carbon fiber polymer-matrix structural composite under flexture," *Carbon*, vol. 45, pp. 1606–1613, 2007.

[46] D. Chung, "Self-monitoring structural materials," *Materials Science and Engineering*, vol. R22, pp. 57–78, 1998.

[47] W. Li, J. Yuan, A. Dichiara, Y. Lin, and J. Bai, "The use of vertically aligned carbon nanotubes grown on *sic* for *in situ* sensing of elastic and plastic deformation in electrically percolative epoxy composites," *Carbon*, vol. 50, pp. 4291–4301, 2012.

[48] D. Wang and D. Chung, "Through-thickness stress sensing of a carbon fiber polymer-matrix composite by electrical resistance measurement," *Smart Materials and Structures*, vol. 16, pp. 1320–1330, 2007.

[49] S. Wang and D. Chung, "Self-sensing of flexural strain and damage in carbon fiber polymer-matrix composite by electrical resistance measurement," *Carbon*, vol. 44, no. 13, pp. 2739–2751, 2006.

[50] N. Angelidis, C. Wei, and P. Irving, "The electrical resistance response of continuous carbon fibre composite laminates to mechanical strain," *Composites: Part A*, vol. 35, pp. 1135–1147, 2004.

[51] S. Wicks, R. G. de Villoria, and B. Wardle, "Interlaminar and intralaminar reinforcement of composite laminates with aligned carbon nanotubes," *Composites Science and Technology*, vol. 70, pp. 20–28, 2010.

[52] N. Yamamoto, A. Hart, E. Garcia, S. Wicks, H. Duong, A. Slocum, and B. Wardle, "High-yield growth and morphology control of carbon nanotubes on ceramic fibers for multifunctional enhancement of structural composites," *Carbon*, vol. 47, pp. 551–560, 2009.

[53] S. Ashley. (Aug 2009) Nanostitching, 'fuzzy fibers' boost composites through-plane properties. http://www.sae.org/mags/sve/6763. SAE International.

[54] J. Blanco, E. Garcia, R. G. de Villoria, and B. Wardle, "Limiting mechanisms of mode i interlaminar toughness of composites reinfprced with aligned carbon nanotubes," *Journal of Composite Materials*, vol. 43, p. 825, April 2009.

[55] E. Garcia, B. Wardle, A. Hart, and N. Yamamoto, "Fabrication and multifunctional properties of a hybrid laminate with aligned carbon ananotubes grown *in situ*," *Composite Science and Technology*, vol. 68, pp. 2034–2041, 2008.

[56] S. Wicks, R. G. de Villoria, and B. Wardle, "Tomographic electrical resistance-based damage sensing in nano-engineered composite structures," in *51st AIAA/ASME/ASCE/AHS/ASC Structures, Structural Dynamics, and Materials Conference*, 2010.

[57] R. G. de Villoria, N. Yamamoto, A. Miravete, and B. Wardle, "Enhanced thermographic damage detection enabled by multifunctional nanoengineered composite laminates," in *52nd AIAA/ASME/ASCE/AHS/ASC Structures, Structural Dynamics, and Materials Conference*, 2011.

[58] (Feb 2013) Hexply 8552 product data. http://www.hexcel.com/Resources/DataSheets/Prepreg-Data-Sheets/8552_eu.pdf. Hexcel Composites.

[59] E. Garcia, A. Hart, B. Wardle, A. Slocum, and D. Shim, "Aligned carbon nanotube reinforcement of graphite/epoxy ply interfaces," in *16th International Conference on Composite Materials*, Kyoto, Japan, 2007.

[60] (2013) 1/8 in quasi-isotropic carbon fiber high modulus uni sheet. http://www.dragonplate.com//ecart/product.asp?pID=5148&cID=166. Allred and Associated, Inc.

[61] (2013) Sem paint, paste aerosol - conductive adhesive. http://www.tedpella.com/SEMmisc_html/SEMpaint.htm. Ted Pella, Inc.

[62] J. Chambers, "Durability testing of an aircraft structural health monitoring system," Master's thesis, Massachusetts Institute of Technology, September 2006.

A Appendix: Sample Summary

Below are tables listing further information on samples tested.

Table 2: Summary of relevant set up and sample types with notation used; inches are used to comply with units common in the aerospace industry; HP = Hexcel w/ CNT patch; HC = Hexcel, no CNT Patch, control; DP = DragonPlate w/ CNT patch, DC = DragonPlate, no CNT patch, control; FFRP = Fuzzy Fiber Reinforced Plastic

Sample	Probe Configuration	Thickness (in)	Notes	Testing Notes
HP1	grid	0.0820		slippage, pulled 3x
HP2	grid	0.0845		slippage, pulled 2x
HP3	grid	0.0830		
HP4	grid	0.0830		
HP5	grid	0.0805		
HC1	grid	0.0810		slippage, pulled 1x
HC2	grid	0.0825		
HC3	vertical	0.0815		pulled 1mm/min
HC4	horizontal	0.0800		
DP1	vertical	0.1285		
DP2	vertical	0.1285		
DP3	vertical	0.1285		
DP4	vertical	0.1285		
DP5	vertical	0.1300		
DP6	horizontal	0.1280		
DP7	horizontal	0.1280		
DP8	horizontal	0.1285		
DP9	horizontal	0.1280		longer cable used
DP10	horizontal	0.1290		longer cable used
DC1	vertical	0.1285		
DC2	vertical	0.1290		
DC3	horizontal	0.1295		pins started to deform
DC4	horizontal	0.1290		pins started to deform
FFRP1	grid	0.0845	1% weight gain	
FFRP2	grid	0.1030	2% weight gain	
FFRP3	grid	0.1218	3% weight gain	
FFRP4	grid	0.1065	4% weight gain	
FFRP5	grid	0.1035	2% weight gain	

- Slippage indicates that during testing the samples were not clamped with sufficient pressure, such that during tensile testing, the Instron would simply pull the off the grips on the samples without straining the sample itself. The number of times pulled indicates the number of cycles that particular sample went through before proper gripping pressure was obtained.
- Towards the end of testing, the cables and pins used to read resistances off the samples would deform with further testing. This was because as the samples failed, it would cause the pins to disconnect from

the sample violently. During some tests, this required replacing the cable with longer cables. Samples tested with longer cable have higher initial resistances due to the contributions of the cables to the resistance of the system.

- Sample HC3 was pulled at four times the strain rate of other samples.

Table 3: Summary of manufacturing parameters for FFRP samples; listed weight gains are listed in order used during the lay-up process; weight gains are on the order of 0.1 g, excluding the catalyst

Sample	Weight Gain Target	Actual Weight Gain per Layer (wt%)
V	1% weight gain	1.34, 0.72, 1.67, 1.35, 1.56, 1.26
W	2% weight gain	2.08, 1.86, 2.27, 2.10, 1.98, 2.11
X	3% weight gain	2.96, 2.74, 3.14, 2.89, 2.79, 2.94
Y	4% weight gain	3.79, 3.58, 3.83, 3.50, 3.93, 3.73
Z	2% weight gain	2.27, 1.74, 2.14, 2.00, 1.90, 1.96

Table 4: Summary of mechanical and testing data for each sample; R_o is the initial resistance; ultimate load is taken to be the maximum load during the test; elongation is translated from time of fracture in seconds using strain rate as conversion factor

Sample	Avg R_o [min, max](Ohm)	St. Dev R_o	Fracture Load (kN)	Fracture Elong. (mm)
HP1	3.14 [2.53, 3.67]	0.57	30230	2.63
HP2	3.77 [3.42, 4.88]	0.33	26324	2.10
HP3	3.19 [2.86, 3.85]	0.24	27178	2.16
HP4	5.88 [5.37, 6.82]	0.37	28494	2.32
HP5	8.13 [6.86, 11.31]	1.01	26254	2.08
HC1	8.00 [5.17, 13.39]	2.42	26049	(slippage)
HC2	8.21 [5.57, 15.07]	2.19	26533	2.01
HC3	11.29 [6.39, 17.92]	3.45	29321	2.90
HC4	4.11 [3.57, 5.63]	0.52	26.95	2.19
DP1	4.62 [3.16, 6.31]	0.93	40386	3.67
DP2	2.95 [2.31, 6.13]	1.09	39886	3.03
DP3	2.73 [2.06, 5.68]	1.01	38711	2.89
DP4	2.87 [2.29, 5.92]	1.05	41995	3.49
DP5	2.82 [2.31, 5.58]	0.95	57693	5.58
DP6	2.38 [1.98, 4.04]	0.58	41397	3.28
DP7	2.30 [1.88, 4.17]	0.65	41009	3.20
DP8	2.31 [1.86, 4.03]	0.61	40820	3.18
DP9	2.91 [2.53, 4.83]	0.66	41427	3.20
DP10	3.12 [2.51, 4.63]	0.62	60687	6.05
DC1	2.47 [2.12, 4.41]	N/A	60.22	4.02
DC2	2.68 [2.45, 3.26]	N/A	61.17	4.10
DC3	2.21 [2.14, 2.41]	N/A	57.09	3.27
DC4	3.11 [2.39, 8.74]	N/A	57.17	3.66
FFRP1	7.76 [5.37, 12.57]	2.18	9.31	1.03
FFRP2	8.50 [6.25, 13.56]	1.80	9.96	1.10
FFRP3	8.93 [5.93, 14.16]	2.19	10.49	1.20
FFRP4	5.59 [4.20, 8.75]	1.19	9.85	1.10
FFRP5	7.64 [5.59, 11.42]	1.52	9.67	1.07

B Appendix: CVD furnace growths and characterization for FFRP samples

Below are the growth conditions and resulting morphology of CNTs grown for the FFRP samples.

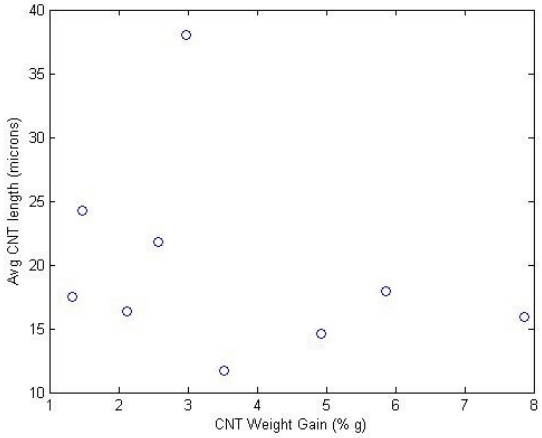

Average CNT length and percent weight gains

With accompanying SEM images

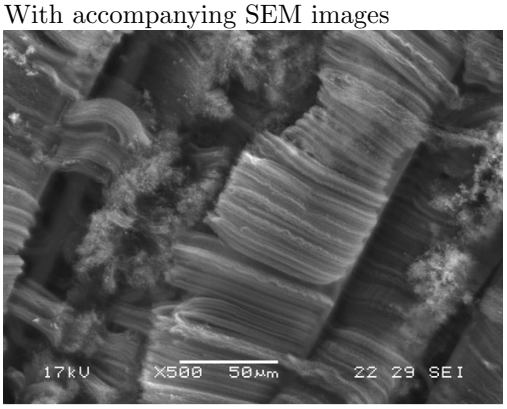

Figure 29: SEM image of the grown CNTs in a ply of the FFRP samples, 1.47wt% gain

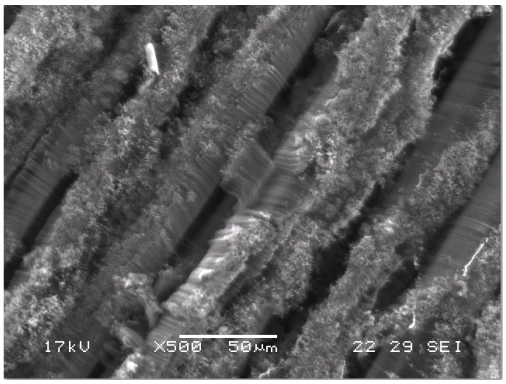

SEM image of the grown CNTs in a ply of the FFRP samples, 2.89wt% gain

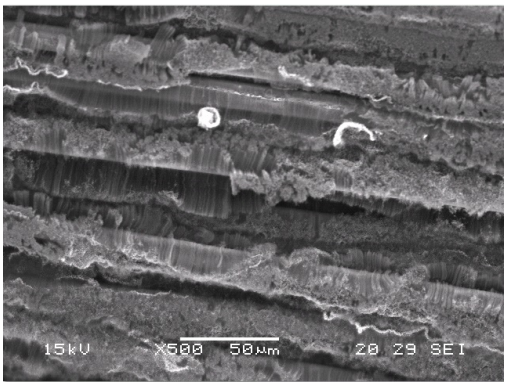

SEM image of the grown CNTs in a ply of the FFRP samples, 5.84wt% gain

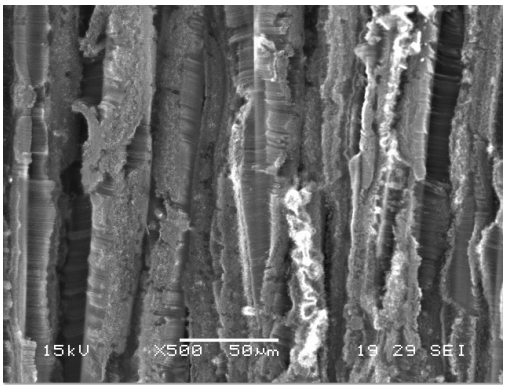

SEM image of the grown CNTs in a ply of the FFRP samples, 7.87wt% gain

C Appendix: Sample Plots of Correlation between Stress Curve and Measured Resistance Changes

Below are plots for the remaining samples not shown in the results and discussion. Due to the volume of possible plots, plots from each sample is shown below with minimal premature probe failure. Plots are listed in order sample listings in Appendix A. Far field measurements are those taken away from the stress concentration and near field measuremnets are those taken in direct vicinity of the stress concentration. All plots are overlay of strain (% mm/mm) with percent change in resistance (% Ohms) and stress (MPa).

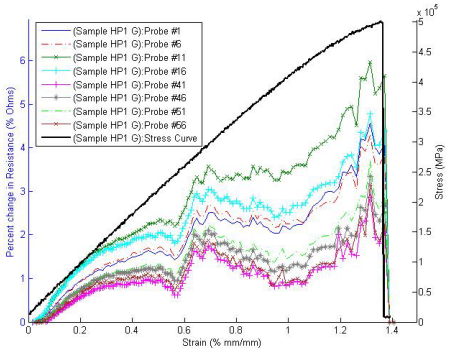

Figure 30: Sample HP 1, far field measurements

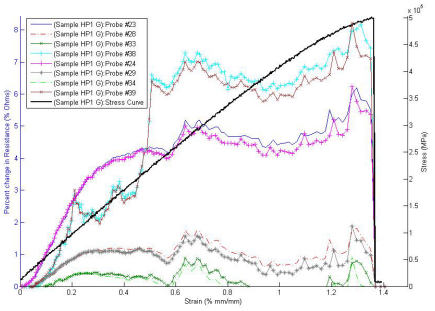

Figure 31: Sample HP1, near field measurements

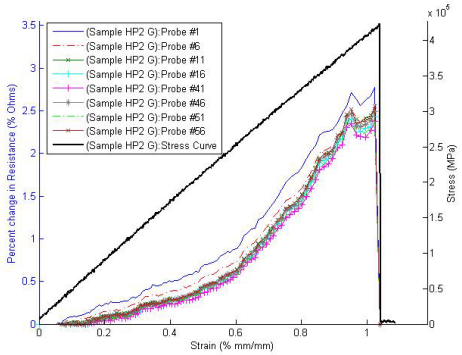

Figure 32: Sample HP2, far field measurements

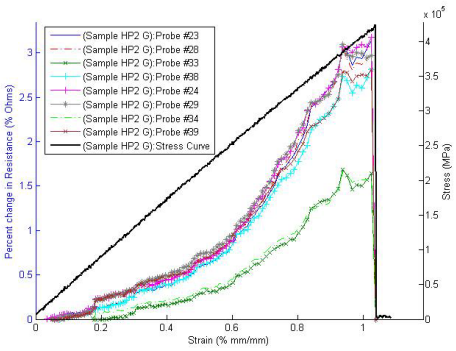

Figure 33: Sample HP2, near field measurements

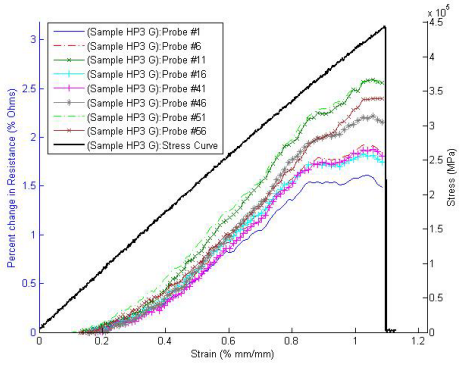

Figure 34: Sample HP3, far field measuremnets

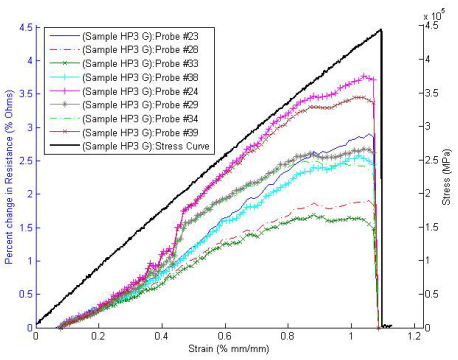

Figure 35: Sample HP3, near field measurements

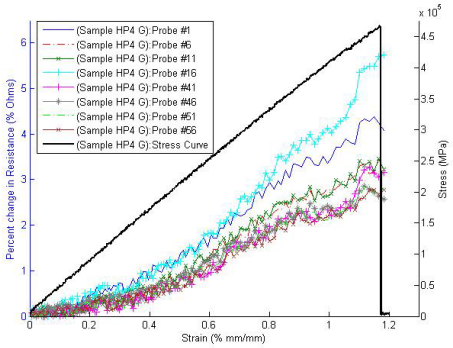

Figure 36: Sample HP4, far field measuremnets

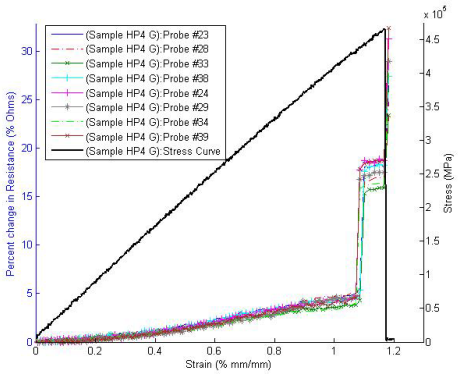

Figure 37: Sanple HP4, near field measurements

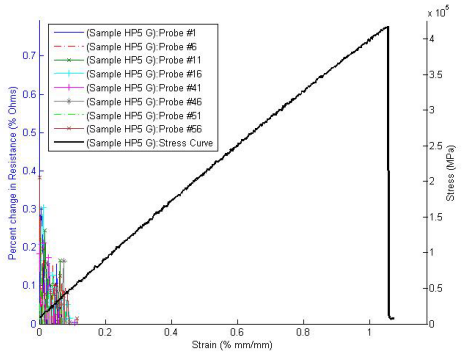

Figure 38: Sample HP5, far field measuremnets

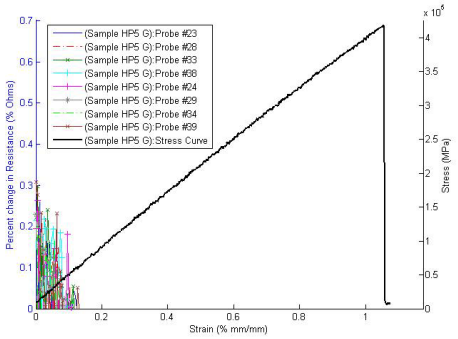

Figure 39: Sample HP5, near field measurements

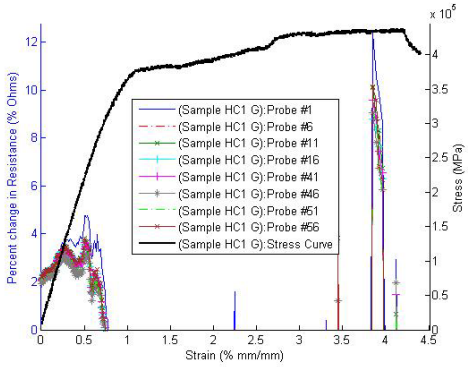

Figure 40: Sample HC1, far field measurements

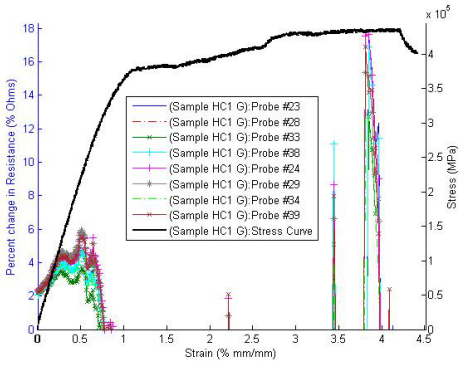

Figure 41: Sample HC1, near field measurements

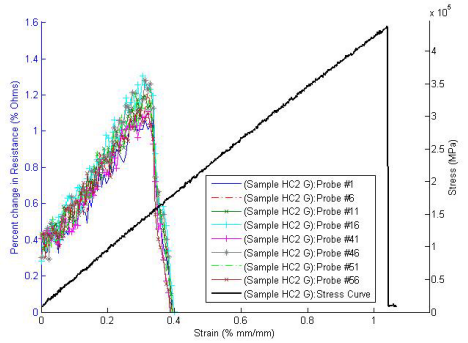

Figure 42: Sample HC2, far field measurement

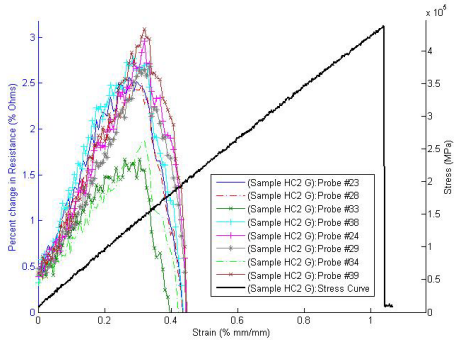

Figure 43: Sample HC2, near field measurements

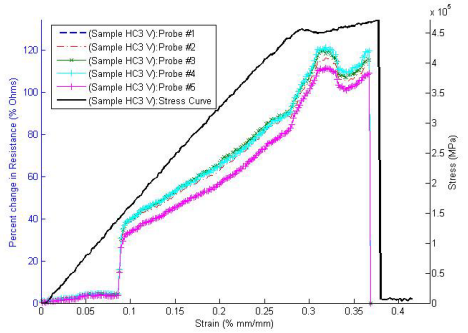

Figure 44: Sample HC3, far field measurements

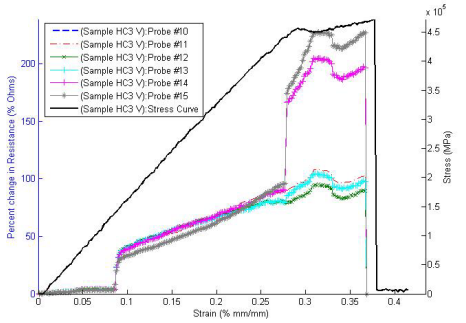

Figure 45: Sample HC3, near field measurements*

*Sample HC3 was initially pulled at 1mm/min and then subsequently at 0.25mm/min, and so the change in compliance in the above curve is due to testing error

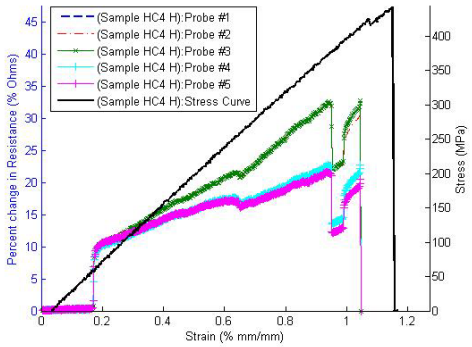

Figure 46: Sample HC4, far field measurements

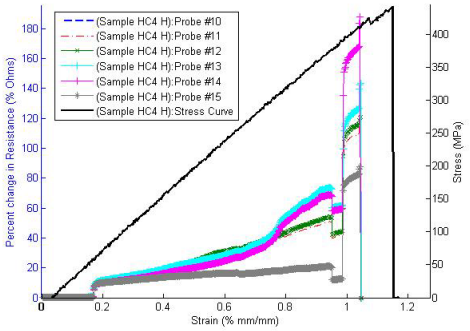

Figure 47: Sample HC4, near field measurements

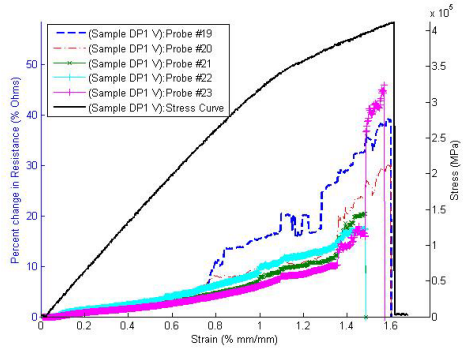

Figure 48: Sample DP1, far field 2 measurements

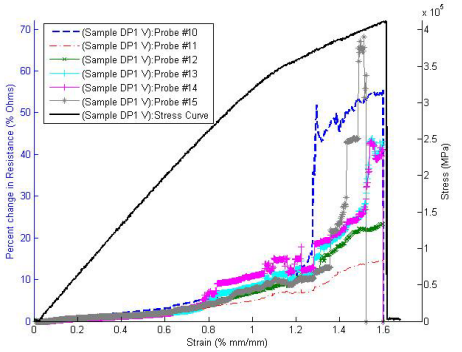

Figure 49: Sample DP1, near field measurements

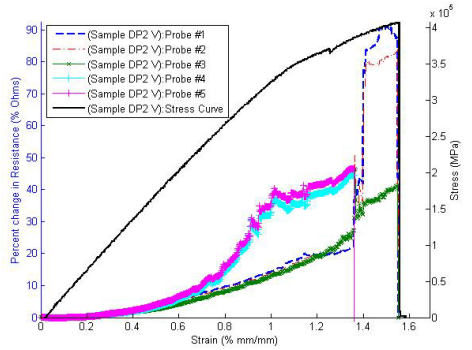

Figure 50: Sample DP2, far field 1 measurements

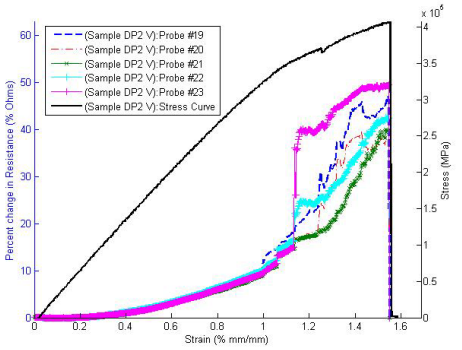

Figure 51: Sample DP2, far field 2 measurements

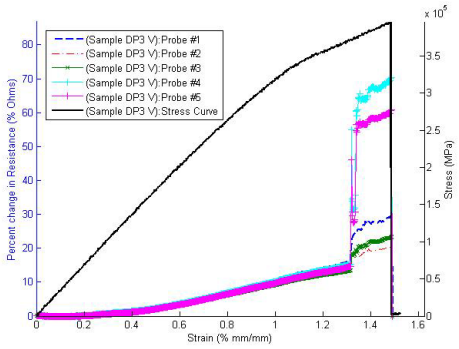

Figure 52: Sample DP, far field 1 measurements

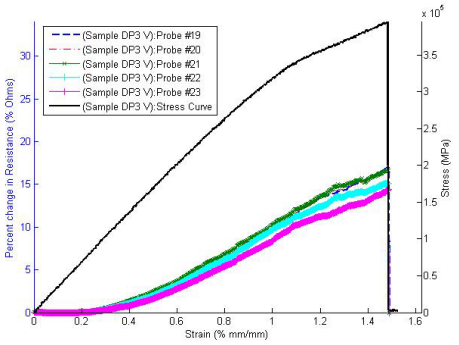

Figure 53: Sample DP3, far field 2 measurements

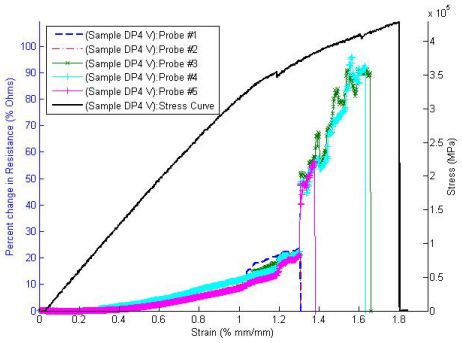

Figure 54: Sample DP4, far field 1 measurements

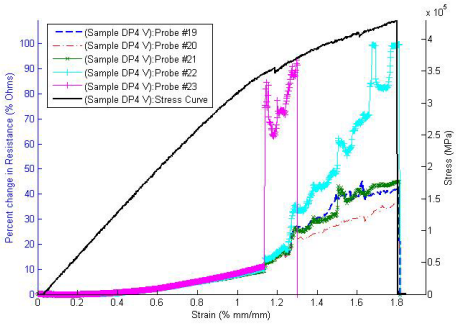

Figure 55: Sample DP4, far field 2 meausurements

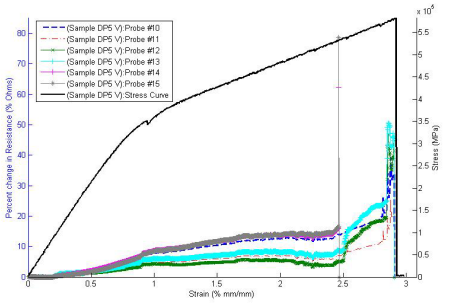

Figure 56: Sample DP5, near field measurements

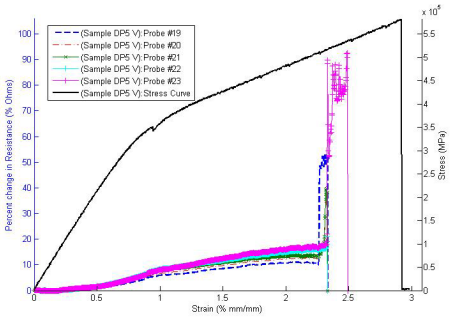

Figure 57: Sample DP5, far field 2 measurements

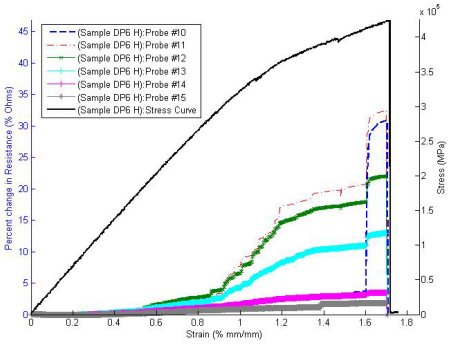

Figure 58: Sample DP6, near field measurements

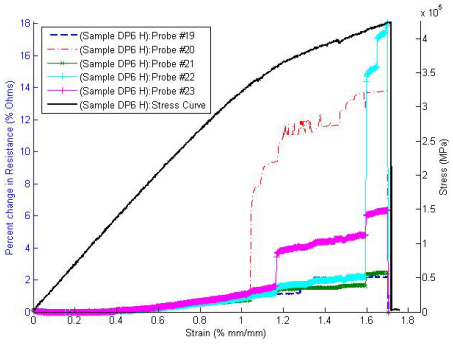

Figure 59: Sample DP6, far field 2 measurements

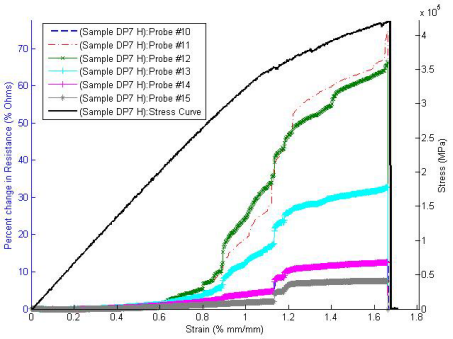

Figure 60: Sample DP7, near field measurements

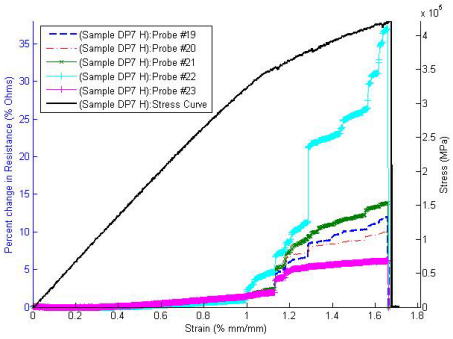

Figure 61: Sample DP7, far field 2 measurements

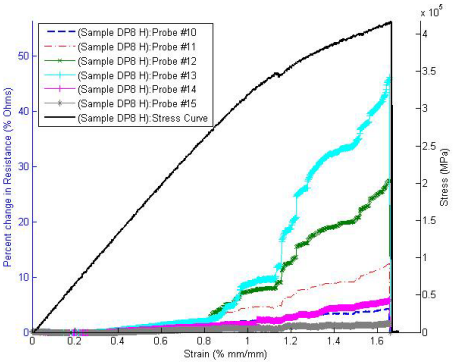

Figure 62: Sample DP8, near field measurements

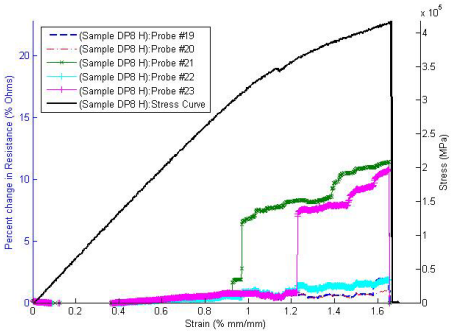

Figure 63: Sample DP8, far field 2 measurements

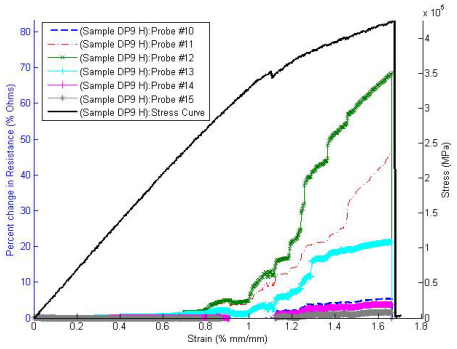

Figure 64: Sample DP9, near field measurements

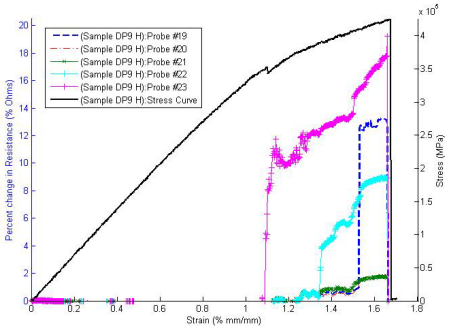

Figure 65: Sample DP9, far field 2 measurements

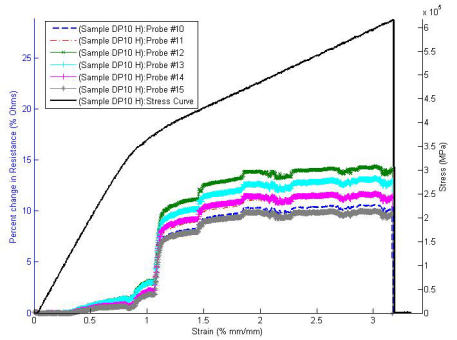

Figure 66: Sample DP10, near field measurements

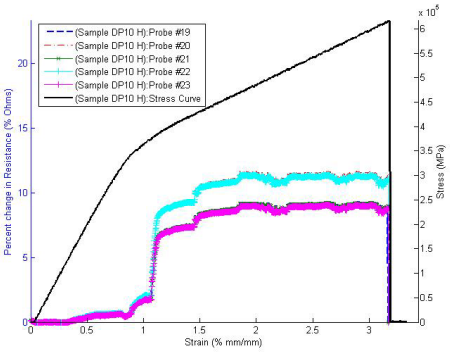

Figure 67: Sample DP10, far field 2 measurements

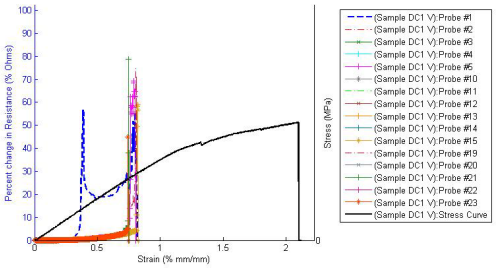

Figure 68: Sample DC1, all probes

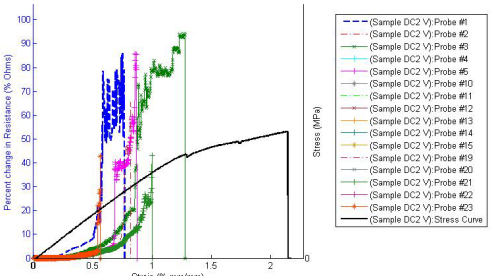

Figure 69: Sample DC2, all probes

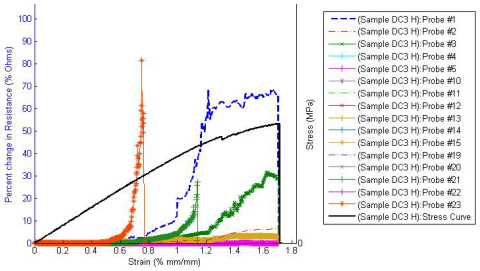

Figure 70: Sample DC3, all probes

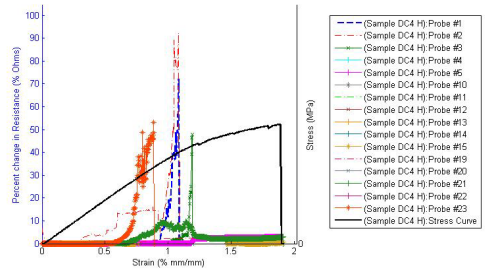

Figure 71: Sample DC4, all probes

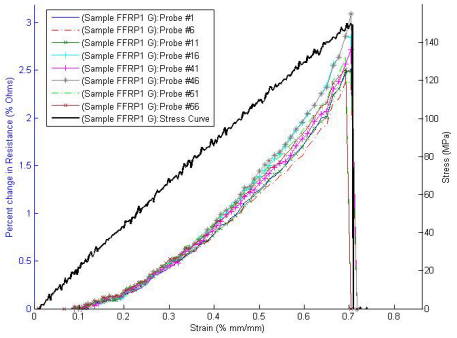

Figure 72: Sample FFRP1, far field measurements

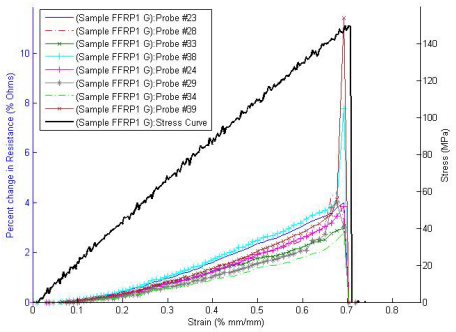

Figure 73: Sample FFRP1, near field measurements

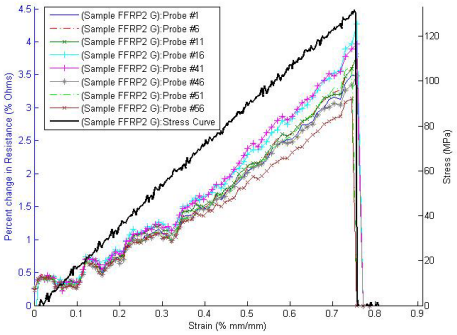

Figure 74: Sample FFRP2, far field measurements

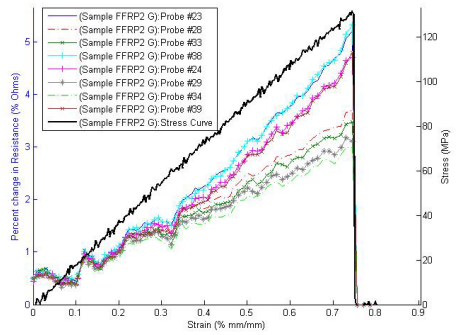

Figure 75: Sample FFRP2, near field measurements

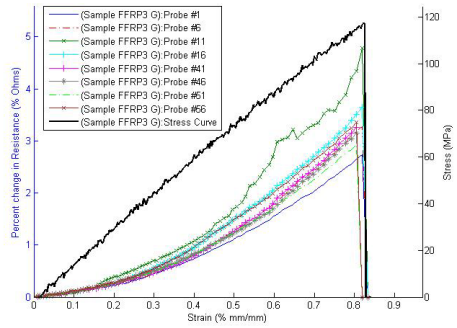

Figure 76: Sample FFRP3, far field measurements

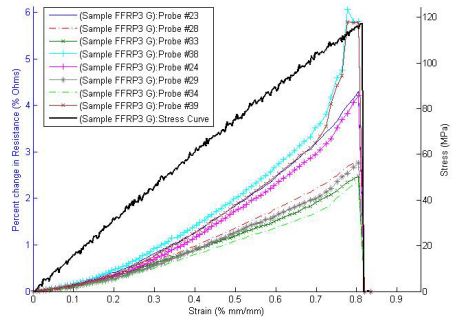

Figure 77: Sample FFRP3, near field measurements

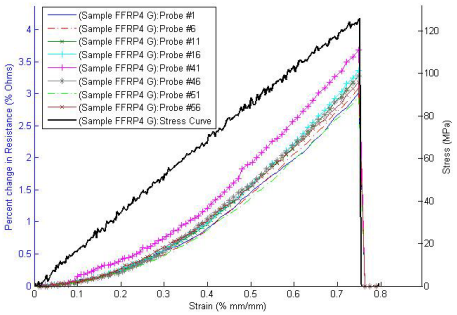

Figure 78: Sample FFRP4, far field measurements

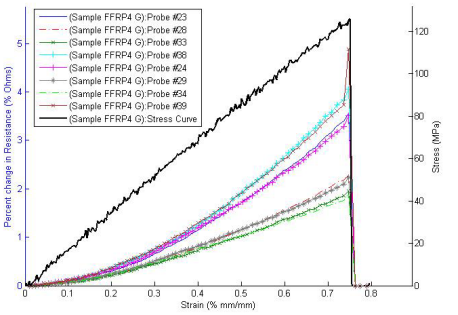

Figure 79: Sample FFRP4, near field measurements

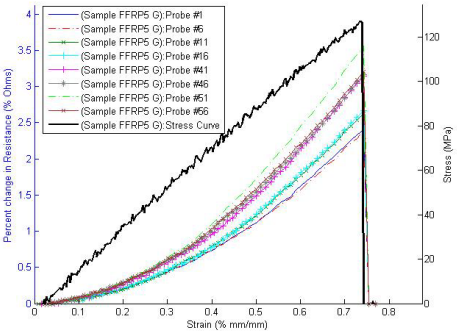

Figure 80: Sample FFRP5, far field measurements

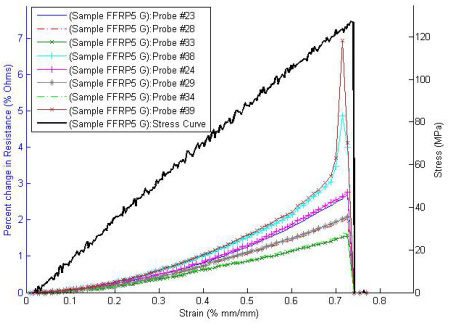

Figure 81: Sample FFRP5, near field measurements